

## TRIAXIAL GALAXIES WITH CUSPS

DAVID MERRITT AND TEMA FRIDMAN

Department of Physics and Astronomy, Rutgers University, Piscataway, NJ 08855

Rutgers Astrophysics Preprint No 160

### ABSTRACT

We have constructed fully self-consistent models of triaxial galaxies with central density cusps. The triaxial generalizations of Dehnen's (1993) spherical mass models are presented, which have densities that vary as  $r^{-\gamma}$  near the center and  $r^{-4}$  at large radii. We computed libraries of  $\sim 7000$  orbits in each of two triaxial models with  $\gamma = 1$  ("weak cusp") and  $\gamma = 2$  ("strong cusp"); these two models have density profiles similar to those of the "core" and "power-law" galaxies observed by HST. Both mass models have short-to-long axis ratios of 1:2 and are maximally triaxial. The major orbit families and their associated periodic orbits were mapped as a function of energy. A large fraction of the orbits in both model potentials are stochastic, as evidenced by their non-zero Liapunov exponents. We show that most of the stochastic orbits in the strong-cusp potential diffuse relatively quickly through their allowed phase-space volumes, on time scales of  $10^2 - 10^3$  dynamical times. Stochastic orbits in the weak-cusp potential diffuse more slowly, often retaining their box-like shapes for  $10^3$  dynamical times or longer.

Attempts to construct self-consistent solutions using just the regular orbits failed for both mass models. Quasi-equilibrium solutions that include the stochastic orbits exist for both models; however, real galaxies constructed in this way would evolve near the center due to the continued mixing of the stochastic orbits. We attempted to construct more nearly stationary models in which stochastic phase space was uniformly populated at low energies. These "fully mixed" solutions were found to exist only for the weak-cusp potential; as much as  $\sim 1/3$  of the mass near the center of these models could be placed on stochastic orbits without destroying the self-consistency. No significant fraction of the mass could be placed on fully-mixed stochastic orbits in the strong-cusp model, demonstrating that strong triaxiality can be inconsistent with a high central density.

Our results suggest that chaos is a generic feature of the motion in realistic triaxial potentials, but that the presence of chaos is not necessarily inconsistent with the existence of stationary triaxial configurations.

## 1. INTRODUCTION

A central question in the study of elliptical galaxies is the extent to which nature can construct equilibrium stellar systems that are not axisymmetric. Schwarzschild (1979, 1982) presented two numerical models of equilibrium triaxial galaxies, with and without figure rotation, and Statler (1987) showed that self-consistent equilibria exist for the fully integrable, “perfect” mass models presented by Kuzmin (1973) and by de Zeeuw & Lynden-Bell (1985). Triaxial stellar systems also seem to form naturally in  $N$ -body simulations (e.g. Aarseth & Binney 1978; Wilkinson & James 1982).

Real elliptical galaxies look rather different from the idealized models of Schwarzschild (1979) and Statler (1987), which had large, constant-density cores in which the orbital motion is essentially harmonic. Recent ground based (Moller, Stiavelli & Zeilinger 1995) and space telescope (Crane *et al.* 1993; Jaffe *et al.* 1994; Ferrarese *et al.* 1994; Lauer *et al.* 1995) observations demonstrate that early-type galaxies essentially never have constant-density cores; the stellar surface brightness always continues to rise into the smallest observable radius. (Systematic deviations of elliptical galaxy core profiles from the “isothermal” law were noted as early as 1985 by Kormendy from ground-based observations.) Ferrarese *et al.* (1994) and Lauer *et al.* (1995) divide elliptical galaxies into two classes based on their nuclear properties, which Lauer *et al.* call “core” and “power-law” galaxies. “Core” galaxies exhibit an obvious break in the surface brightness profile at some radius  $R_b$ ; inward of this break, the profile turns down to a shallow inner power law  $\Sigma(R) \propto R^{-\alpha}$ ,  $\alpha \approx -0.1 \pm 0.1$ . “Power-law” galaxies show roughly a single power-law profile throughout their inner regions with  $\alpha \approx -0.8 \pm 0.2$ . Power-law galaxies are of lower average luminosity than core galaxies, but steep surface brightness profiles are seen in galaxies with a very wide range of luminosities, from  $M_V \approx -15$  to  $M_V \approx -22$  (Kormendy *et al.* 1995).

The division of elliptical galaxies into two groups based on their surface brightness profiles is probably unnecessary once one takes into account the effects of projection on the luminosity density profiles. Nonparametric deprojection of the Lauer *et al.* surface brightness data (Merritt & Fridman 1995) demonstrates that the so-called “core” galaxies, like the “power-law” galaxies, also exhibit power-law cusps in their *spatial* densities. These galaxies appear in projection to have “cores” only because the logarithmic slopes of their central luminosity density profiles lie between  $-1$  and  $0$ , and power-law cusps shallower than  $1/r$  do not appear as power laws when seen in projection (e.g. Dehnen 1993, Fig. 1). Lauer *et al.*’s “power-law” galaxies, by contrast, have spatial density cusps with power-law indices that lie between  $-1$  and  $-2$ ; cusps this steep retain their power-law character even when projected against the outer layers of the galaxy. Gebhardt *et al.* (1996) have recently shown that there is no qualitative difference between the luminosity density profiles of the two types of galaxy, and in fact both can be well fit by a single family of parametric models, such as the family of Dehnen (1993) that is used here (Kormendy, private communication). Thus, power-law density cusps are a generic feature of elliptical galaxies, and the fact that some ellipticals have surface brightness profiles that flatten at

small radii appears to be an artifact of projection onto the plane of the sky.

This universal, power-law character of elliptical galaxy nuclei is not wholly surprising in view of the fact that  $N$ -body simulations of structure formation often produce systems with power-law density profiles (e.g. Crone, Evrard & Richstone 1994).

It has long been known that the addition of a central mass concentration to an otherwise integrable triaxial potential can have profound effects on at least one family of orbits, the boxes, which fill a region that includes the center. Gerhard and collaborators (Gerhard & Binney 1985; Gerhard 1987) showed that nuclear black holes or density cusps will subject stars on box orbits to deflections that can destroy two of their three integrals of motion. The evolution of such an orbit can be described as a series of near-random transitions from one box orbit to another; after a long time, the orbit would be expected to uniformly fill the phase-space region corresponding to all trajectories, with a given energy, that pass near the center. Gerhard & Binney (1985) pointed out that the time-averaged density distribution of such an orbit is likely to be rounder than that of a typical box orbit, which suggests that stationary triaxial configurations may not exist when the central mass concentration is too high. None of these objections apply to axisymmetric models, for which all the orbits conserve one component of the angular momentum and therefore avoid the center. Thus Gerhard & Binney (1985) suggested that triaxial galaxies with strong central mass concentrations would evolve in the direction of axisymmetry, at least near their centers, as the box orbits gradually lost their distinguishability.

One complication to this picture is the existence of stable box-like orbits. Periodic orbits are dense in any phase space, and periodic orbits that avoid the center can remain stable even in the presence of a central cusp or black hole. Examples of periodic orbits that (like box orbits) begin on an equipotential surface and pass close to the center are the 2:1 planar orbits, the “bananas;” the 3:2 “fish;” the 4:3 “pretzels;” etc. If they are stable, such periodic orbits can generate families of regular orbits that might contribute strongly to a self-consistent solution. Schwarzschild and collaborators (Miralda-Escudé & Schwarzschild 1989; Lees & Schwarzschild 1992) investigated the existence and stability of these “boxlets” in the principal planes of a variety of non-integrable triaxial models, including the logarithmic potential that corresponds to an inverse-square dependence of density on radius. Based on the variation of boxlet shape with model flattening, these authors concluded that strongly flattened, triaxial models might not exist. Pfenniger & de Zeeuw (1989) reached a similar conclusion.

Kuijken (1993) constructed self-consistent, scale-free models of triaxial disks, and Schwarzschild (1993), extending the work of Richstone (1980, 1982, 1984) and Levison & Richstone (1987), found self-consistent solutions for a set of three-dimensional scale-free ( $\rho \propto r^{-2}$ ) mass models with various axis ratios, designed to represent dark halos. The orbital motion in Schwarzschild’s models was largely stochastic, somewhat more so than suggested by earlier surface-of-section studies in the principal planes of scale-free models (e.g. de Zeeuw & Pfenniger 1988; Miralda-Escudé & Schwarzschild 1989). (We demonstrate below that this enhanced stochasticity can be traced to the vertical instability

of the planar periodic orbits. Motion in the principal planes turns out to be a poor guide to the three-dimensional motion.) Schwarzschild (1994) found that self-consistent solutions could not always be constructed using only the regular orbits, especially for flatter models. However solutions that included the stochastic orbits could always be found. We will use the term “quasi-equilibrium” to describe solutions like Schwarzschild’s that contain distinguishable stochastic orbits. In a quasi-equilibrium model, the continued mixing of the stochastic orbits would produce a slow evolution of the model figure, especially near the center. Schwarzschild estimated that this evolution would not seriously compromise the self-consistency of his models, at least over time scales corresponding to  $\sim 10^2$  orbital periods that are relevant to the outer parts of galactic halos. Orbital periods near the center of a galaxy with a cusp can be much shorter than 1% of a Hubble time, however, and the evolution of stochastic orbits would be expected to have more serious consequences there.

Here we present the first, fully self-consistent, non-scale-free models of triaxial galaxies with central density cusps. Motivated by the space telescope observations described above, we investigate two mass models with densities that increase as  $1/r$  (“weak-cusp”) and  $1/r^2$  (“strong-cusp”) near the center (§2); both have minor-to-major axis ratios of 1:2 and are maximally triaxial. We find (§3) that the phase space corresponding to orbits that touch an equipotential surface, and that would be classified as “box” orbits in an integrable potential, is largely stochastic for both mass models. We investigate the time scales for diffusion of these stochastic orbits and show that they are relatively short, roughly  $10^3$  dynamical times, in the model with the  $1/r^2$  cusp (§4). We then attempt (§5) to construct self-consistent solutions that include the stochastic orbits in various ways. Solutions that exclude the stochastic orbits do not exist for either mass model - the regular orbits are sufficiently rare, and limited enough in their shapes, that they can not reproduce the model density everywhere. Quasi-equilibrium solutions, in which the stochastic orbits are treated like the regular orbits, exist for both mass models; however, a galaxy constructed in this way would evolve in shape, especially near the center, as the stochastic orbits continued to diffuse through their allowed phase-space regions.

We therefore attempted to construct models that exclude the stochastic orbits at low energies, where the diffusion time scales are short, or that populate the stochastic orbits in an approximately time-independent way. We found that these “fully mixed” solutions exist for the weak-cusp model, in the sense that the stochastic orbits throughout the central regions of the model could be replaced by a single “orbit” at every energy representing a steady-state population of phase space without destroying the self-consistency. A galaxy constructed in this way would evolve only very slowly due to the continued mixing of stochastic orbits at large energies. Fully-mixed solutions could not be found for the model with the  $1/r^2$  cusp, however, demonstrating that strong central mass concentrations are sometimes inconsistent with triaxiality. The smaller variety of self-consistent solutions for the strong-cusp model is probably due to the paucity of regular orbit families in this potential; hence, more weight is placed on the stochastic orbits.

All of our self-consistent solutions are dominated by stochastic orbits. Second in importance are the tube orbits, which typically contribute about half of the total mass; the “boxlets,” the regular remnants of the box orbits, are dynamically almost insignificant. Our results highlight the likely importance of chaos in the phase-space structure of strongly triaxial stellar systems. We show (§5) how Jeans’s theorem can be generalized to include systems containing both regular and stochastic orbits; thus, chaos is not necessarily inconsistent with fully stationary triaxial equilibria. However our attempts at model-building demonstrate that fully stationary equilibria do not exist for every choice of triaxial mass model, including some that are quite similar in appearance to real galaxies. Furthermore, nature may not be inclined to populate the stochastic orbits in just the right way to guarantee full equilibrium, especially at large radii where mixing time scales for stochastic orbits are long. Thus, slow evolution may be a generic property of triaxial stellar systems (§6).

## 2. DENSITY, POTENTIAL, FORCES

The mass models considered in this study are the triaxial generalizations of the spherical models first discussed in detail by Dehnen (1993), and more recently by Carollo (1993) and Tremaine *et al.* (1994). Our models have a mass density

$$\rho(m) = \frac{(3 - \gamma)M}{4\pi abc} m^{-\gamma} (1 + m)^{-(4-\gamma)}, \quad 0 \leq \gamma < 3 \quad (1a)$$

with

$$m^2 = \frac{x^2}{a^2} + \frac{y^2}{b^2} + \frac{z^2}{c^2}, \quad a \geq b \geq c \geq 0, \quad (1b)$$

and  $M$  the total mass. The mass is stratified on ellipsoids with axis ratios  $a : b : c$ ; the  $x$  [ $z$ ] axis is the long [short] axis. The parameter  $\gamma$  determines the slope of the central density cusp. For  $\gamma = 0$  the model has a finite-density core; for  $\gamma > 0$  the central density is infinite. The strongest cusp that we will consider here has  $\gamma = 2$ , i.e.  $\rho \propto m^{-2}$  at small radii. At large radii, all models have  $\rho \propto m^{-4}$ .

The functional form (1), with a suitable choice for  $\gamma$ , has been shown to be a good approximation to the luminosity densities of a number of elliptical galaxies. Jaffe (1983) advocated the choice  $\gamma = 2$ , and Hernquist (1990) suggested  $\gamma = 1$ . As discussed above, recent space telescope observations demonstrate that elliptical galaxies and bulges exhibit a variety of cusp strengths,  $\gamma \lesssim 2$ . Few if any galaxies are observed to have  $\gamma \approx 0$ , i.e. a constant-density core.

The gravitational potential of a body in which  $\rho = \rho(m^2)$  may be written

$$\Phi(\mathbf{x}) = -\pi Gabc \int_0^\infty \frac{[\psi(\infty) - \psi(m)] d\tau}{\sqrt{(\tau + a^2)(\tau + b^2)(\tau + c^2)}} \quad (2a)$$

(Chandrasekhar 1969, Theorem 12), with

$$\psi(m) = \int_0^{m^2} \rho(m'^2) dm'^2 \quad (2b)$$

and

$$m^2(\tau) = \frac{x^2}{a^2 + \tau} + \frac{y^2}{b^2 + \tau} + \frac{z^2}{c^2 + \tau}. \quad (2c)$$

We find, for  $\gamma \neq 2$ ,

$$\Phi(\mathbf{x}) = -\frac{GM}{2(2-\gamma)} \int_0^\infty \frac{\left[1 - (3-\gamma) \left(\frac{m}{1+m}\right)^{2-\gamma} + (2-\gamma) \left(\frac{m}{1+m}\right)^{3-\gamma}\right] d\tau}{\sqrt{(\tau+a^2)(\tau+b^2)(\tau+c^2)}}, \quad (3a)$$

while for  $\gamma = 2$

$$\Phi(\mathbf{x}) = -\frac{GM}{2} \int_0^\infty \frac{\left[\log\left(\frac{1+m}{m}\right) - \frac{1}{1+m}\right] d\tau}{\sqrt{(\tau+a^2)(\tau+b^2)(\tau+c^2)}}. \quad (3b)$$

In the spherical limit, these expressions reduce to those in Dehnen (1993):

$$\begin{aligned} \Phi(r) &= -\frac{GM}{(2-\gamma)a} \left[1 - \frac{(r/a)^{2-\gamma}}{(1+r/a)^{2-\gamma}}\right], \quad \gamma \neq 2, \\ &= -\frac{GM}{a} \log\left(1 + \frac{a}{r}\right), \quad \gamma = 2. \end{aligned} \quad (4)$$

The central value of the potential is divergent for  $\gamma = 2$ .

The gravitational forces are

$$-\frac{\partial\Phi}{\partial x_i} = -(3-\gamma)G \left(\frac{x_i}{2}\right) \int_0^\infty \frac{m^{-\gamma} d\tau}{(a_i^2 + \tau)(1+m)^{4-\gamma} \sqrt{(\tau+a^2)(\tau+b^2)(\tau+c^2)}}, \quad i = 1, 2, 3, \quad (5)$$

with  $a_1 \equiv a$ ,  $a_2 \equiv b$ ,  $a_3 \equiv c$ . In the spherical case, we have

$$-\frac{\partial\Phi}{\partial r} = -\frac{GM}{a^2} \left(\frac{r}{a}\right)^{1-\gamma} \left(1 + \frac{r}{a}\right)^{\gamma-3}. \quad (6)$$

Below we construct self-consistent models based on just two choices for the parameters  $a, b, c$  and  $\gamma$ . Both mass models have the same set of axis ratios:

$$\frac{c}{a} = \frac{1}{2}, \quad T \equiv \frac{a^2 - b^2}{a^2 - c^2} = \frac{1}{2}, \quad (7)$$

i.e. both are “maximally triaxial” ellipsoids with major-to-minor axis ratios of 2:1. Model 1, which we will call the “weak cusp” model, has  $\gamma = 1$ , while model 2, the “strong cusp” model, has  $\gamma = 2$ . According to equation (6), the central force diverges as  $r^{-1}$  in the strong cusp model, while in Model 1 the central force is finite but nonzero.

Henceforth we adopt units in which the total mass  $M$ , the  $x$ -axis scale length  $a$ , and the gravitational constant  $G$  are unity.

The expressions (3) and (5) are improper integrals and not very suitable for numerical computation. The potential integrals were rewritten using the substitution  $s = (1+\tau)^{-1/2}$ . For  $\gamma \neq 2$  this yields the proper integral

$$\Phi = -\frac{1}{2-\gamma} \int_0^1 \frac{\left[1 - (3-\gamma) \left(\frac{m}{1+m}\right)^{2-\gamma} + (2-\gamma) \left(\frac{m}{1+m}\right)^{3-\gamma}\right] ds}{\sqrt{[1 + (b^2 - 1)s^2][1 + (c^2 - 1)s^2]}}, \quad (8a)$$

with

$$m^2(s) = s^2 \left[ x^2 + \frac{y^2}{1 + (b^2 - 1)s^2} + \frac{z^2}{1 + (c^2 - 1)s^2} \right]. \quad (8b)$$

For  $\gamma = 2$  we have

$$\Phi = - \int_0^1 \frac{\left[ \log \left( \frac{(1+m)s}{m} \right) - \frac{1}{1+m} \right] ds}{\sqrt{[1 + (b^2 - 1)s^2][1 + (c^2 - 1)s^2]}} + C, \quad (9a)$$

$$C = \int_0^1 \frac{\log t \, dt}{\sqrt{[1 + (b^2 - 1)t^2][1 + (c^2 - 1)t^2]}}. \quad (9b)$$

The substitution  $s = a_i(a_i^2 + \tau)^{-1/2}$  gives for the components of the force

$$F_i = -\frac{\partial \Phi}{\partial x_i} = -(3-\gamma) \frac{x_i}{a_i} \int_0^1 \frac{s^2 ds}{m^\gamma (1+m)^{4-\gamma} \sqrt{(a_i^2 + A_1 s^2)(a_i^2 + A_2 s^2)}}, \quad (10a)$$

with

$$m^2(s) = s^2 \left( \frac{x^2}{a_i^2 + C_1 s^2} + \frac{y^2}{a_i^2 + C_2 s^2} + \frac{z^2}{a_i^2 + C_3 s^2} \right). \quad (10b)$$

The constants are

$$\begin{aligned} i = 1 : & A_1 = b^2 - 1 & A_2 = c^2 - 1 & C_1 = 0 & C_2 = b^2 - 1 & C_3 = c^2 - 1 \\ i = 2 : & A_1 = c^2 - b^2 & A_2 = 1 - b^2 & C_1 = 1 - b^2 & C_2 = 0 & C_3 = c^2 - b^2 \\ i = 3 : & A_1 = 1 - c^2 & A_2 = b^2 - c^2 & C_1 = 1 - c^2 & C_2 = b^2 - c^2 & C_3 = 0. \end{aligned} \quad (10c)$$

The transformed integrals were evaluated numerically using the NAG routine D01AHF.

The derivatives of the forces were needed when computing the Liapunov exponents, as described below (§3). These are:

$$\frac{\partial^2 \Phi}{\partial x_i^2} = -\frac{F_i}{x_i} - \frac{3-\gamma}{a_i} \left( \frac{x_i}{a_i} \right)^2 \int_0^1 \frac{(\gamma + 4m_i) s^4 ds}{m_i^{\gamma+2} (1+m_i)^{5-\gamma} \sqrt{(a_i^2 + A_1 s^2)(a_i^2 + A_2 s^2)}}, \quad (11a)$$

$$\frac{\partial^2 \Phi}{\partial x_i \partial x_j} = -\frac{(3-\gamma) x_i x_j}{a_i} \int_0^1 \frac{(\gamma + 4m_i) s^4 ds}{m_i^{\gamma+2} (1+m_i)^{5-\gamma} [a_i^2 + (a_j^2 - a_i^2) s^2]^{3/2} \sqrt{(a_i^2 + (a_k^2 - a_i^2) s^2)}}, \quad (12b)$$

Because we forced our models to have equidensity surfaces that are precisely ellipsoidal, our expressions for the forces and the potential could not be reduced below one-dimensional integrals and were therefore expensive to compute. We justify this expense on the grounds that real elliptical galaxies have isophotes that are also very nearly elliptical. Much modelling in the past has been based on simpler expressions for the forces that correspond to strongly dimpled mass distributions.

In our adopted units, one unit of time corresponds to:

$$1.49 \times 10^6 \text{yr} \left( \frac{M}{10^{11} M_\odot} \right)^{-1/2} \left( \frac{a}{1 \text{kpc}} \right)^{3/2}. \quad (13)$$

We will often present elapsed times in units of an energy-dependent “dynamical time” or “orbital time”  $T_D$ , defined as the period of the (nearly circular) 1:1 resonant orbit in the  $x - y$  plane. Table 1 gives the period of this orbit in model units as a function of energy for the two adopted mass models. The energy values in this table are equal to those used for the construction of the orbit library, as described below.

### 3. INTEGRATION OF ORBITS AND COMPUTATION OF LIAPUNOV EXPONENTS

Because of the extreme inhomogeneity of these models, the numerical algorithm for integrating the orbits must be extremely accurate and flexible. We used the 7/8 order Runge-Kutta algorithm described by Fehlberg (1968), which incorporates a variable time step in order to maintain a specified accuracy from one integration step to the next. A Fortran version of this routine, RK78, was kindly made available by Dr. Stéphane Udry. The accuracy parameter TOL in all the integrations described below was chosen to be  $10^{-8}$ . We found that a typical orbit conserved energy to a few parts in  $10^9$  over 100 dynamical times with this choice of TOL - a very high level of accuracy.

The potentials considered here are very different from the fully integrable triaxial potentials discussed by Kuzmin (1973), de Zeeuw (1985) and others. We therefore expect that many of the trajectories will conserve only one or two integrals of the motion, rather than the three integrals that characterize fully regular motion. These “stochastic” orbits behave qualitatively differently in many respects from regular orbits and must be treated separately in the construction of self-consistent models, as discussed in greater detail below.

A standard way of detecting and quantifying stochasticity is through computation of the Liapunov characteristic exponents (e.g. Lichtenberg & Lieberman 1992, p. 296). The Liapunov exponents of a trajectory are the mean exponential rates of divergence of trajectories surrounding it. Consider a trajectory in six-dimensional phase space and a nearby trajectory with initial conditions  $\mathbf{x}_0$  and  $\mathbf{x}_0 + \Delta \mathbf{x}_0$ , respectively. These evolve with time yielding a difference vector  $\mathbf{w}(\mathbf{x}_0, t)$  with length  $d(\mathbf{x}_0, t)$ . The mean exponential rate of divergence of two initially close trajectories is

$$\sigma(\mathbf{x}_0, \Delta \mathbf{x}) = \lim_{t \rightarrow \infty} \left( \frac{1}{t} \right) \ln \frac{d(\mathbf{x}_0, t)}{d(\mathbf{x}_0, 0)}. \quad (14)$$



It can be shown that there is a six-dimensional basis  $\{\hat{e}_i\}$  of  $\mathbf{w}$  such that for any  $\mathbf{w}$ ,  $\sigma$  takes on one of the six values

$$\sigma_i(\mathbf{x}_0) = \sigma(\mathbf{x}_0, \hat{e}_i), \quad (15)$$

which are the Liapunov exponents. These can be ordered by size,

$$\sigma_1 \geq \sigma_2 \geq \dots \geq \sigma_6.$$

In the special case of Hamiltonian flow considered here, phase space volume is a conserved quantity and so only three of the Liapunov exponents are independent. It may be shown that

$$\sigma_i = -\sigma_{7-i}, \quad (16)$$

so that we may henceforth restrict our attention to the three positive exponents. Furthermore, for Hamiltonian flow, one of these three exponents will be exactly zero.

Each additional isolating integral aside from the energy causes one more of the Liapunov exponents to be zero. Regular orbits have three isolating integrals and their Liapunov exponents are all zero; the trajectories around such orbits diverge, at best, only linearly. An orbit can be classified as stochastic if the greatest Liapunov exponent is non-zero. A stochastic trajectory that respects only one integral of motion, the energy, will have two non-zero Liapunov exponents; a stochastic orbit that respects two integrals (if such exist) will have only one non-zero Liapunov exponent.

Liapunov characteristic exponents are defined as limiting values over an infinite time interval. Numerical approximations, computed over a finite time interval, are sometimes called “Liapunov characteristic indicators” (e.g. Heggie 1991). We would expect all numerically-computed Liapunov exponents to remain nonzero after a finite integration time.

We computed approximations to the six Liapunov exponents for each of the orbits in our library using the Gram-Schmidt orthogonalization technique described by Benettin *et al.* (1980). A Fortran routine developed by the Geneva Observatory group for carrying out the Benettin *et al.* algorithm, called LIAMAG, was kindly made available by Dr. Stéphane Udry. The technique requires the integration of six perturbation orbits in addition to the orbit under consideration (Udry & Pfenniger 1988). The evolution of the perturbed orbits is determined by the second derivatives of the potential with respect to position; these expressions are given in §2. The time required to integrate an orbit including the six perturbation orbits for 100 orbital times and compute the Liapunov exponents was typically about 2.5 minutes on a DEC Alpha 3000/700 workstation. Computation of the full set of 6840 orbits for one model required about 250 hours.

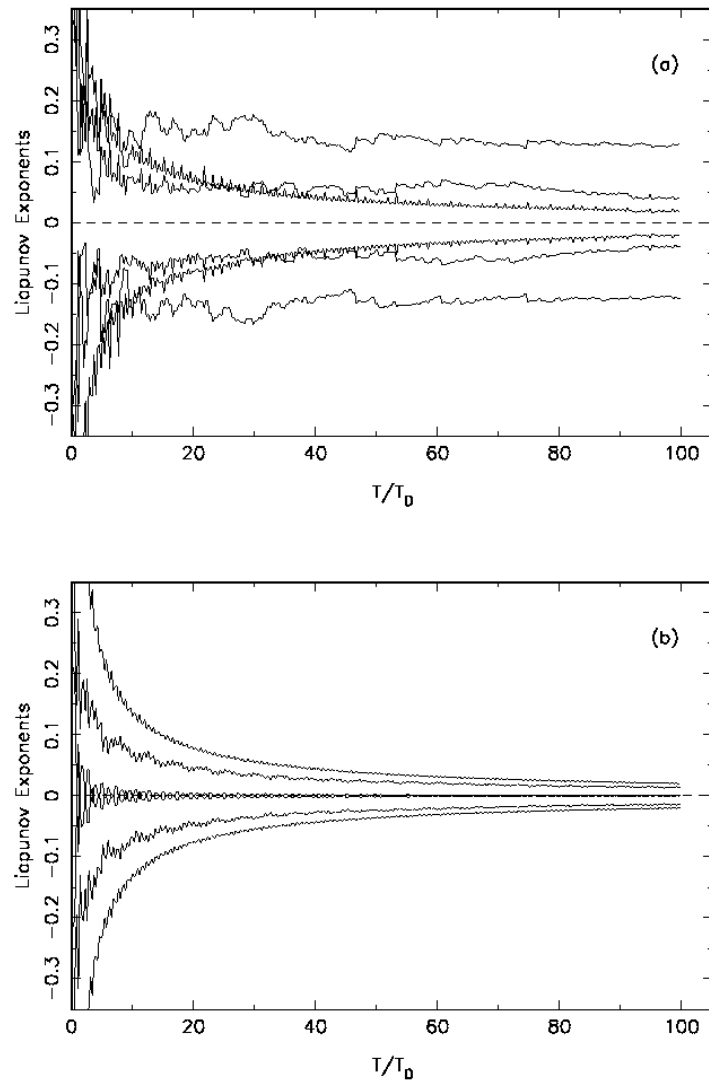


Figure 1. Time dependence of the numerically-computed Liapunov exponents for two orbits in the strong-cusp potential. (a) Stochastic orbit; (b) regular orbit.

Figure 1 shows the numerically-computed Liapunov exponents as a function of time for two orbits, one regular and one stochastic, in the strong-cusp potential. For these two orbits, the time dependence of the exponents is reasonably clear after 100 dynamical times and there is little ambiguity in classifying them as regular or stochastic.

However for many orbits the situation is less clear. The Liapunov exponents are defined as limiting values over an infinite integration time (equation 14). A stochastic

orbit that begins in a region of phase space that is dominated by regular orbits will often remain “trapped” by the surrounding tori for many oscillations, before “breaking out” into the larger stochastic web. Contopoulos & Barbanis (1989) have emphasized that in weakly stochastic regions of phase space, trajectories may need to be integrated for as many as  $10^5$  dynamical times or more in order for the Liapunov exponents to be accurately determined.

Given these difficulties, we adopted the following procedure for distinguishing regular from stochastic orbits. A set of orbits of a single energy was integrated for 100 dynamical times, with initial conditions chosen in a manner to be described below (§4). A histogram was constructed of the positive Liapunov exponents of these orbits: either the largest exponent  $\sigma_1$ ; or the sum of the two largest exponents  $\sigma_1 + \sigma_2$ ; or the sum of all three positive exponents, sometimes called the “Kolmogorov entropy,” or  $h_K$ . (Our finite-time approximations to  $\sigma_3$  tended to be larger for stochastic orbits than for regular ones; after very long integration times, of course,  $\sigma_3 = 0$  even for stochastic orbits.) The histogram based on  $h_K$  was found to be the most effective in distinguishing between regular and stochastic orbits. If the Liapunov exponents were computed accurately, we would expect these histograms to have just two strong peaks: one peak at zero, corresponding to the regular orbits; and one peak at some non-zero value, corresponding to the stochastic orbits. (This expectation is based on the hypothesis - not yet proved in the general case - that all the stochastic trajectories at a given energy in three-dimensional potentials are interconnected via the “Arnold web.”) A spread in values would indicate that the orbits have not been integrated long enough to reach accurate limiting values for the exponents.

Figure 2 shows frequency functions of the Kolmogorov entropy,  $h_k = \sum_{i=1,3} \sigma_i$ , for two sets of 192 orbits computed for 100 dynamical times in the two adopted potentials. (The frequency functions were computed using an adaptive kernel algorithm that yields smooth, continuous curves.) Each orbit began from a point on a single equipotential surface (shell 15 in the nomenclature defined below, §4). The frequency function for orbits in the strong-cusp potential shows a clear peak at small Liapunov numbers, corresponding to the regular orbits, and a broader peak corresponding to the stochastic orbits. In the weak-cusp potential, there is less of a clear distinction between the two categories of orbits.

Clearly our integration time of 100 oscillations is barely sufficient to separate regular from stochastic orbits in the weak-cusp potential, and even in the strong-cusp case, the stochastic orbits show a wide range of Liapunov numbers rather than the single sharp peak that we would expect after an infinite integration time. We therefore explored a number of alternative schemes for more reliably distinguishing between the two sorts of orbits.

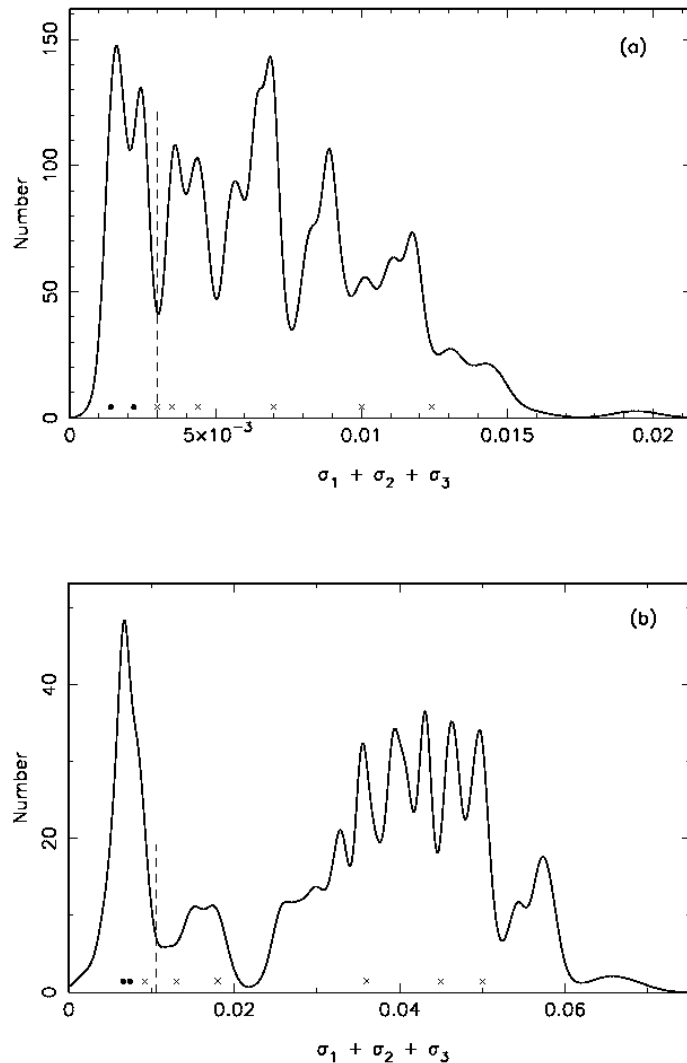


Figure 2. Frequency function of the Kolmogorov entropy,  $h_K = \sum_{i=1}^3 \sigma_i$ , for 192 orbits from shell 15 of the stationary start space. (a) Weak-cusp model; (b) Strong-cusp model. Dashed vertical line is the estimate of the critical  $h_K$  separating regular (left) from stochastic (right) orbits. • and x represent orbits that were integrated for  $10^5$  dynamical times; • = regular, x = stochastic.

We began by integrating a selected set of orbits at several energies for much longer times, up to  $10^5$  orbits, and observing their behavior using the “ergodicity index”  $\Delta$  defined in §4.2. The Liapunov exponents were not computed in order to save time.

These experiments showed that the Liapunov exponents computed after only 100 orbits were a generally accurate indicator of stochasticity, in the sense that a critical value of  $h_K(t = 100T_D)$  could always be found that more-or-less cleanly separated regular from stochastic orbits. Although an occasional orbit with a very low  $h_K$  was found to eventually exhibit stochasticity, by and large the regular and stochastic orbits lay on separate sides of the histogram. Furthermore, the critical value of the Kolmogorov entropy dividing regular from stochastic trajectories was almost always found to lie close to a local minimum in the histogram, typically the first minimum to the right of the peak containing the regular orbits. A plot of critical  $h_K$  versus energy showed a reassuringly smooth and monotonic dependence.

Interestingly, the maximum Liapunov exponent  $\sigma_1$ , or the sum of the two largest exponents  $\sigma_1 + \sigma_2$ , were found to be much less useful for distinguishing between regular and stochastic trajectories in this way. Extra, and useful, information about the stochasticity is apparently contained within the second and third exponents.

(One additional justification for computing the full set of Liapunov exponents might be to determine whether the stochastic orbits respect just a single isolating integral - the energy - or whether some orbits respect two (not three, or one) isolating integrals. In the latter case, we would expect to see just one, non-zero Liapunov exponent. Unfortunately the limited time over which we integrated our orbits did not allow us to reach any very definite conclusions on this question. However most stochastic orbits seemed to have two non-zero exponents after 100 orbital times, implying the existence of no isolating integrals aside from the energy.)

We also looked at a number of more qualitative indicators of stochasticity, including plots of the configuration-space trajectory, the dependence on time of the  $\sigma_i$ , etc. We were struck by how well these different indicators agreed with one another; for instance, a stochastic orbit could almost always be identified as such based on an inspection of its configuration-space trajectory over only a few tens of dynamical times.

Based on these experiments, we are confident that the majority of our orbits have been correctly classified as regular or stochastic, in spite of the rather short integration times. There are undoubtedly some stochastic orbits that we have misclassified as regular, due to “trapping” by nearby tori; some of these stochastic orbits would require an exponentially long time to exhibit their instability. But there are probably few if any regular orbits that we have misclassified as stochastic. Thus, we have probably underestimated slightly the fraction of stochastic orbits in our models.

The orbital times in the outer parts of real galaxies are long enough that many stochastic orbits would behave essentially like regular orbits over astronomical time scales. One might therefore argue that the behavior of a stochastic orbit over time scales much longer than 100 oscillations is of little practical importance to the construction of self-consistent models. However dynamical times become much shorter near the centers of galaxies, particularly galaxies that have central density cusps. For this reason it is important to make a clear distinction between regular and stochastic orbits even if the two classes of orbits

behave similarly on time scales of a few hundred oscillations. We return to the question of diffusion time scales below.

#### 4. ORBIT FAMILIES

For each of the two mass models considered here, 6840 orbits were integrated for 100 dynamical times. We followed Schwarzschild (1993) in assigning initial conditions from one of two sets of starting points: either on an equipotential with zero initial velocity (“stationary”); or in the  $x - z$  plane with  $v_x = v_z = 0$  (“ $X - Z$ ”). Orbits started in the  $x - z$  plane are mostly tube orbits, i.e. they avoid a region near the center of the model. Orbits started on an equipotential surface tend to approach the origin after sufficient time, except for those orbits that lie near to a “centrophobic” periodic orbit. Thus, orbits begun on an equipotential are either stochastic, or else regular “boxlets,” i.e. associated with a stable periodic orbit. As Schwarzschild (1993) argues, these two initial condition spaces probably include most - though strictly speaking not all - of the orbits in the full phase space of a nonrotating triaxial model.

Orbits in both “start spaces” were assigned one of a set of 20 energies, defined as the values of the potential on the  $x$ -axis of a set of ellipsoidal shells - with the same axis ratios as the density - that divide the model into 21 sections of equal mass. These energies are given in Table 1. Thus shell 1 encloses  $1/21$  of the total mass, shell 2 encloses  $2/21$ , etc. Shell 21 lies at infinity. The  $X - Z$  start space was defined as follows. Let  $\theta = \tan^{-1} x/z$  and pick 10 evenly spaced values, from  $\theta = 2.25^\circ$  to  $\theta = 87.75^\circ$ . Compute for each  $\theta$  the zero-velocity limit  $\Phi(x, 0, z) = E$  corresponding to the specified energy. Define a circle in the  $x - z$  plane whose radius is the minimum of the amplitudes of the  $x - y$  or  $y - z$  1:1 periodic orbits at that energy. Then pick 15 equally spaced values at each  $\theta$  at the centers of 15 equal intervals between this circle and the equipotential surface. This scheme yields 150 orbits per shell and minimizes the duplication of orbits that would result from selecting starting points throughout the entire  $x - z$  quadrant.

The stationary start space grid was defined as in Schwarzschild (1993), except that each of the three sectors on an equipotential octant contained only 64 initial points, for a total of 192 orbits per shell.

Orbits were integrated over a time interval equal to 100 dynamical times as given in Table 1. For each orbit, a detailed plot of the following quantities was made:

1. Projection of the orbit onto the  $x = 0$ ,  $y = 0$  and  $z = 0$  planes.
2. Dependence of the  $x$  and  $z$  components of the angular momentum on time.
3. Liapunov exponents (i.e. their numerical approximations) as a function of time.
4. Dependence of the energy conservation on time.

Orbits were then assigned to various categories according to the following scheme. First, the orbit was classified as regular or stochastic. Here we used the procedure outlined above, which required plotting the histogram of Kolmogorov entropies of all the orbits at a given energy and estimating the critical value separating regular from stochastic orbits.

Second, the regular orbits were assigned to one of a set of orbit families. Clearly the possible number of such families is infinite, since periodic orbits of ever higher order are dense in the phase space, and any stable periodic orbit can act as the parent of nearby quasi-periodic orbits. However in practice only a subset of these periodic orbits - though sometimes of surprisingly high order - were found to be important.

#### 4.1. *Regular Orbits*

Our basic set of families included three types: long-axis tubes (L), short-axis tubes (S), and boxes (B). Long-axis tubes have a definite component of angular momentum about the  $x$ -axis; short axis tubes have a definite  $L_z$ ; and boxes have no obvious, nonzero, time-averaged angular momentum components.

When possible, more detailed classifications were made. Long-axis tubes were divided into inner (I) and outer (O) families, following the terminology used by Kuzmin (1973) and de Zeeuw (1985) for tube orbits in fully integrable potentials. Not surprisingly, the presence of a central cusp has little effect on orbits which avoid the center and we found that most long-axis tube orbits fall clearly into the I or O families as defined by those authors.

In the stationary start space, box orbits could often be further grouped into families associated with a stable periodic orbit. The most important of these periodic orbits were identified, and their stability checked, using a Fortran routine written by the Geneva group and kindly made available by S. Udry. Tables 2-5 describe the major families of periodic orbits as a function of energy in the two models. Only the stable periodic orbits are included, with the exception of some unstable low-order resonances in the principal planes, the 2:1 “bananas” and the 3:2 “fish”. Entries for these low-order unstable orbit families are included at shell 1 only. An entry of ‘v’ in the last column denotes instability out of a principal plane, while ‘u’ denotes instability in a more general direction.

Figures 3-6 illustrate the two start spaces for each model. The  $X - Z$  start spaces are similar to those seen in integrable or near-integrable models (e.g. Schwarzschild 1993); most orbits are regular tubes, and fall into one of the three tube families defined above. The stationary start spaces for the weak-cusp model are complex, containing large numbers of orbit families each of which dominates a small part of the space. At large energies the number of important resonances decreases, leaving finally only the 2:1  $x - z$  banana family. In the strong-cusp model, this family is dominant at all energies; the variety of important resonances is smaller than in the weak-cusp model.

The weak-cusp potential is closer than the strong-cusp potential to a fully integrable model, in the sense of having a more nearly constant-density core. In a fully integrable potential, there is only one family of orbits (the boxes) at each energy in stationary start space; the periodic orbits, although they fill the start space densely, generate no new families. Thus we should not be surprised to see a larger number of periodic orbit families in the weak-cusp model, each of which dominates a smaller part of the start space.

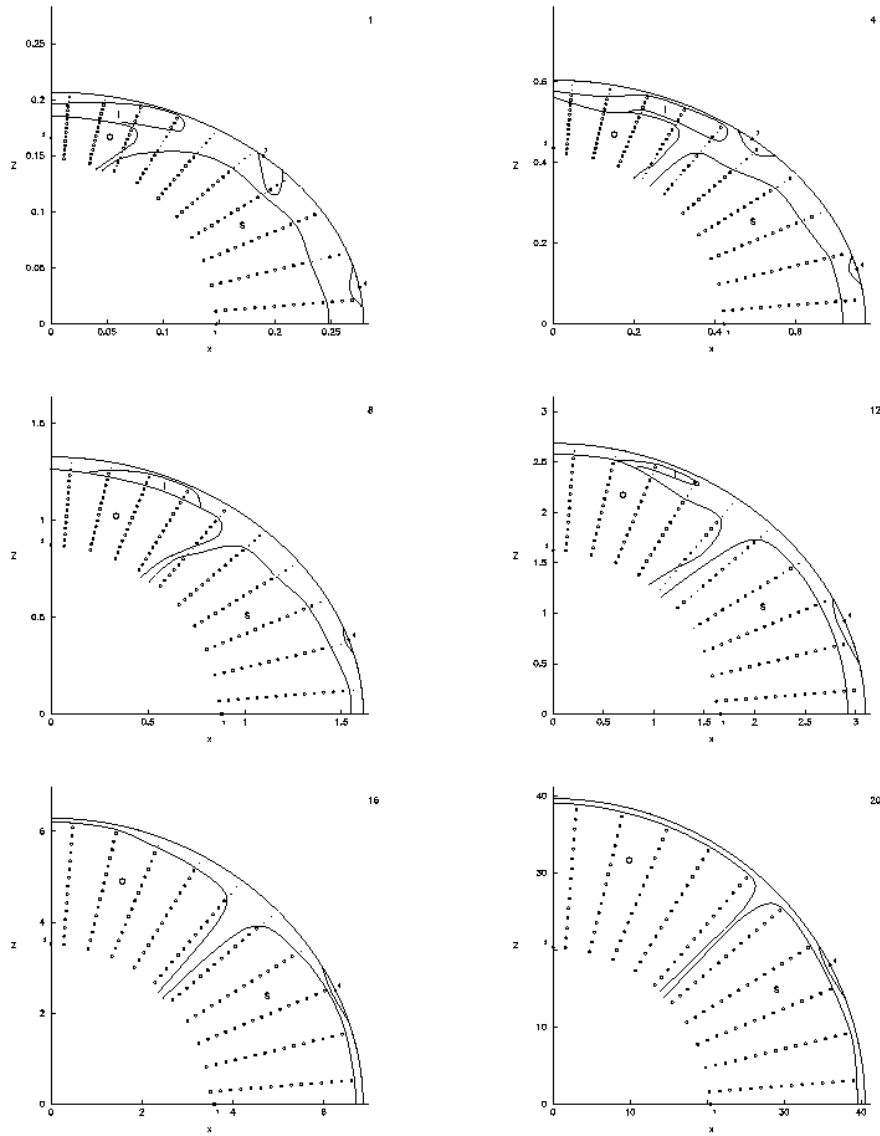


Figure 3. The  $X - Z$  start space at six energies for the weak-cusp model. The numbers in the upper right of each frame denote the shell. The open circles designate the regular orbits, and the small dots the stochastic orbits, in a regular grid of 150 orbits. The symbols S, O and I stand for the three major tube families. The numbered heavy dots represent stable closed orbits for which the resonances are listed in Table 2.



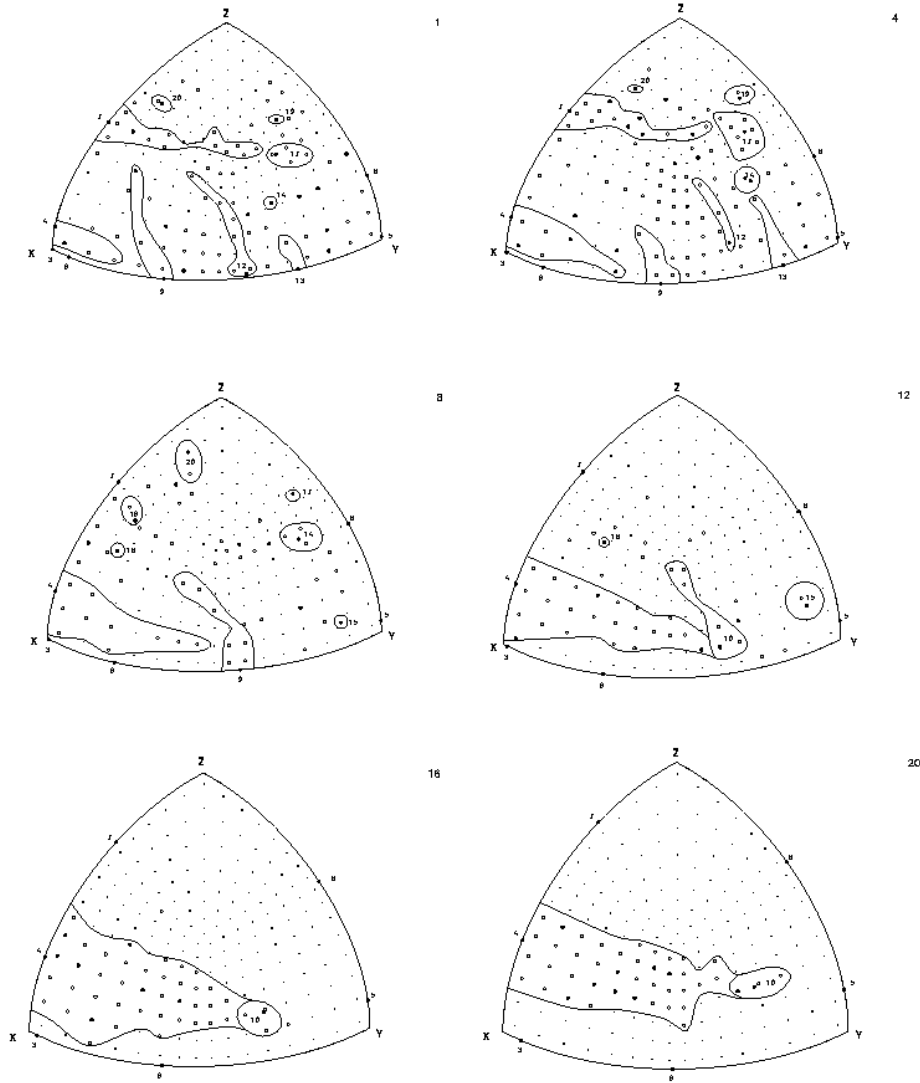


Figure 4. The stationary start space at six energies for the weak-cusp model. The numbers in the upper right of each frame denote the shell. The open circles designate the regular orbits, and the small dots the stochastic orbits, in a regular grid of 192 orbits. The numbered heavy dots represent stable closed orbits for which the resonances are listed in Table 3.

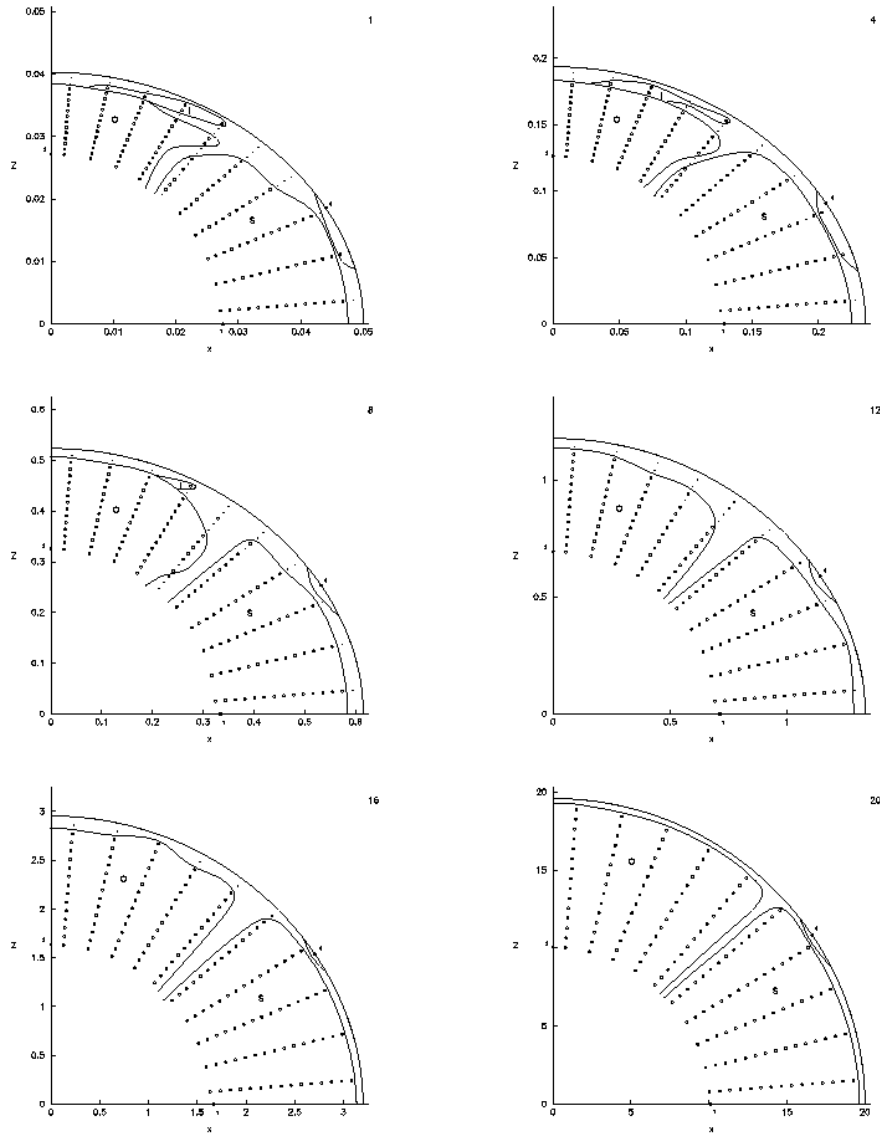


Figure  
5. Like Figure 3, for the strong-cusp model. Resonant orbits are listed in Table 4.

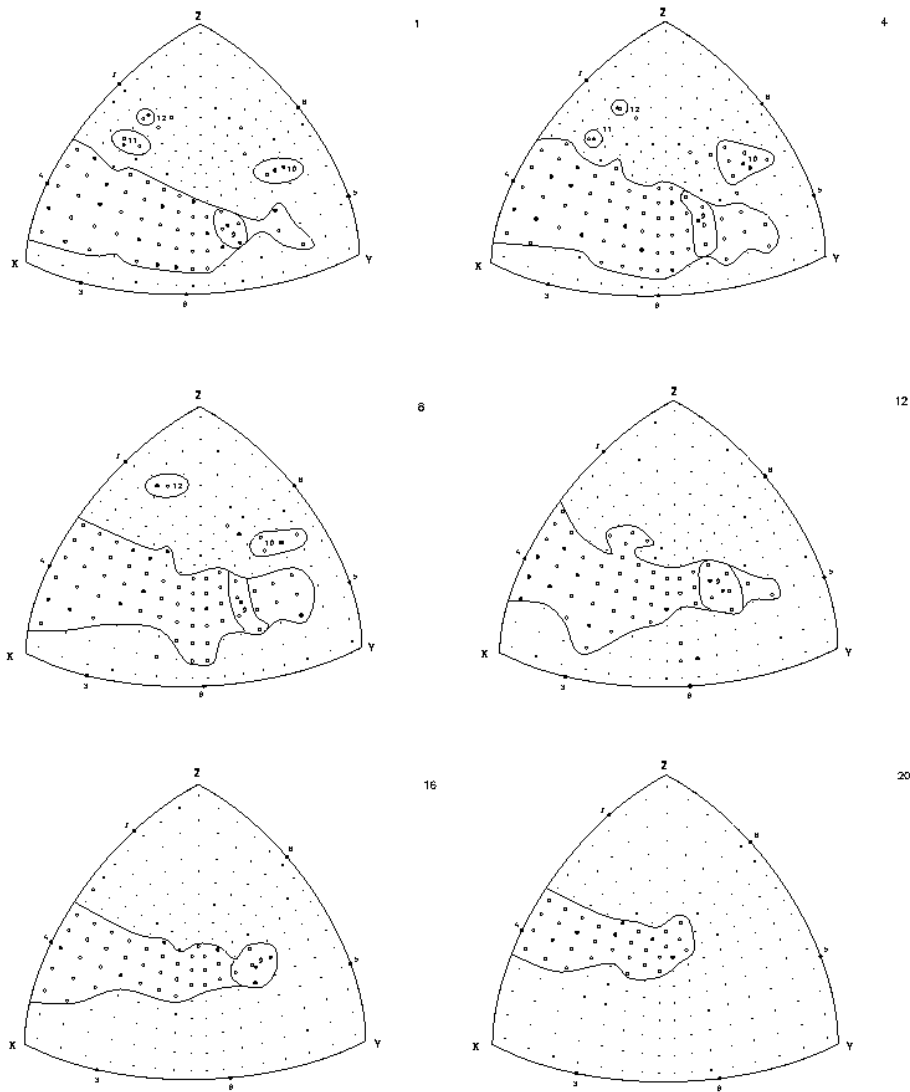


Figure 6. Like Figure 4, for the strong-cusp model. Resonant orbits are listed in Table 5.

As we will see, the greater variety of regular orbit types in the weak-cusp model makes it easier to find a self-consistent solution that does not strongly weight the stochastic orbits.

Our classification scheme differs in one important respect from that of Schwarzschild (1993), who assigned even some stochastic orbits to families associated with stable periodic orbits (see his Figs. 4 and 5) - presumably on the basis that many stochastic orbits behave like regular orbits over short time intervals. We chose instead to maintain a clear distinction between regular and stochastic orbits, for the reasons outlined above. In practice, of course, some misclassifications will always occur.

#### 4.2. *Stochastic Orbits*

A large fraction of the orbits at all energies from the stationary start space, and a significant fraction of the orbits from the  $X - Z$  start space, were found to be stochastic in both model potentials. Figure 7 shows the fraction of stochastic orbits as a function of shell number for both models. We emphasize that these fractions can not be simply related to phase-space volumes; nevertheless they give a crude picture of the relative importance of stochasticity at different energies. In the weak-cusp model, the stochastic fraction is  $\sim 0.6$  at low energies in the stationary start space and increases to  $\sim 0.8$  at high energies. In the strong-cusp model, this fraction is relatively constant with energy at  $\sim 0.8$ . The fraction of stochastic orbits in the  $X - Z$  start space is lower in both models: roughly 0.1 - 0.2 at low energies, falling to zero at high energies. We interpret the much lower fraction of stochastic orbits from the  $X - Z$  start space in terms of the smaller perturbing effect of the central cusp: orbits begun from the  $X - Z$  plane are mostly tubes, which avoid the center.

Remarkably, the overall fraction of stochastic orbits is approximately the same in the two models, even though the strength of the cusp - which is presumably responsible for generating much of the stochasticity - is very different in the two potentials. However the numerically-computed Liapunov exponents are smaller by a factor of a few (after scaling by the dynamical time) in the weak-cusp model than in the strong-cusp model. Thus the stochastic orbits in the weak-cusp model should take longer to diffuse through phase space than those in the strong-cusp model. We now discuss the consequences of these different instability rates for the behavior of stochastic orbits over longer time scales.

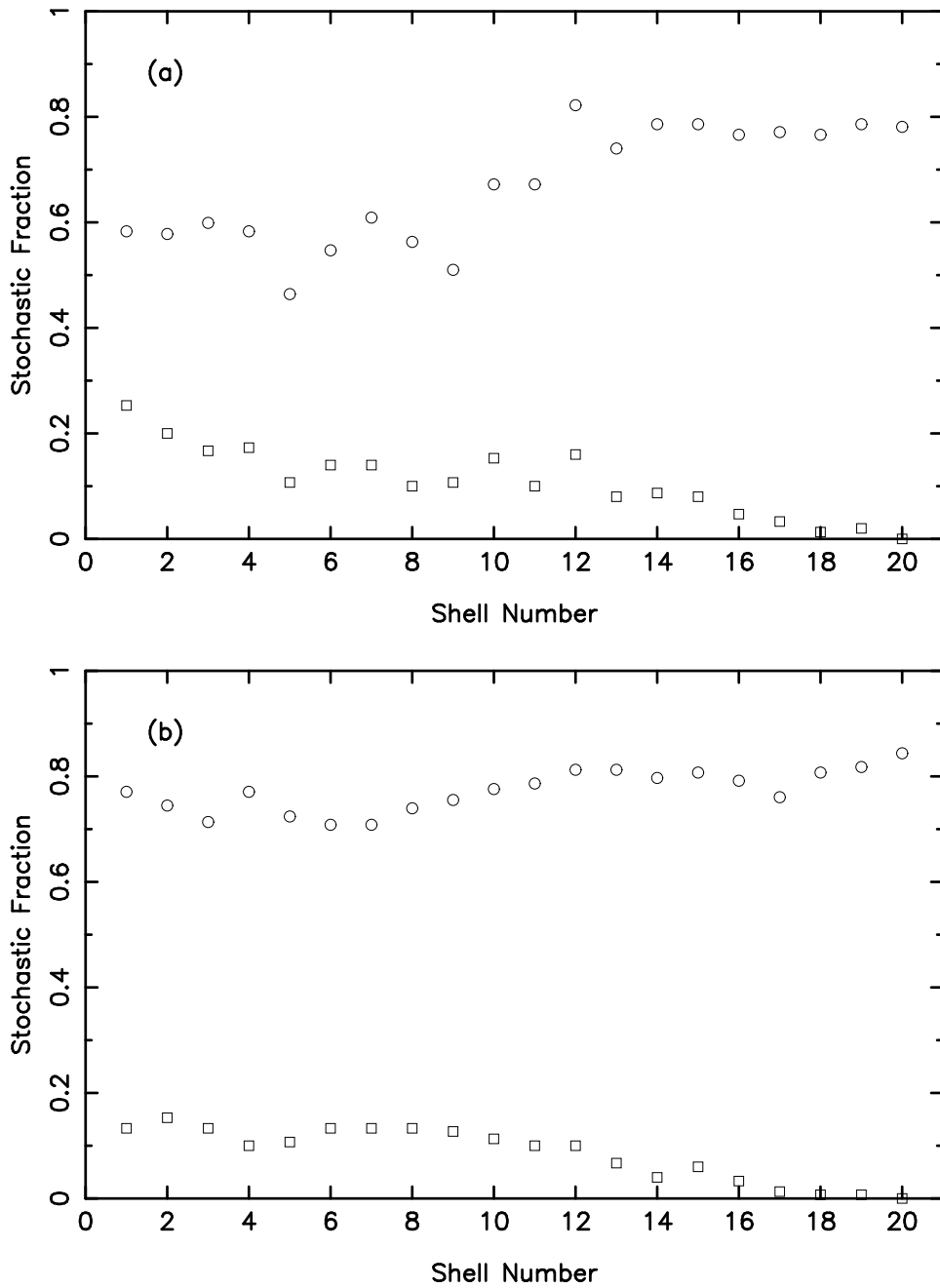


Figure 7. Fraction of stochastic orbits per shell in the orbit libraries, in the weak-cusp (a) and strong-cusp (b) models. Circles: stationary start space; squares:  $X-Z$  start space.

It is generally believed that the stochastic trajectories of a given energy in a system with three degrees of freedom are connected into a single complex network, the so-called

“Arnold web” (e.g. Lichtenberg & Liebermann 1992, p. 380 ff). For any initial condition within the stochastic region, a trajectory will eventually come infinitesimally close to every point in phase space consistent with energy conservation. This diffusion is sometimes broken into two parts: a relatively fast diffusion, resulting from the essentially random motion of the phase point throughout a stochastic layer surrounding an unstable periodic orbit; and a slow diffusion, the “Arnold diffusion,” that links together parts of stochastic phase space that are nearly isolated by the presence of invariant tori associated with regular orbits (Arnold 1964; Lichtenberg & Lieberman 1992, p. 386). The time scale for the fast diffusion can be as short as a dynamical time, particularly if the phase space is globally stochastic so that the trajectory wanders essentially randomly over the entire energy surface. An example is the Hénon-Heiles (1964) potential at high energies. The slower, Arnold diffusion is usually associated only with systems of three or more spatial dimensions, where the topology of phase space implies that the stochastic trajectories are fully interconnected. Arnold diffusion takes place on a time scale that can be arbitrarily long if the phase space is nearly integrable (Chirikov 1979), and it is usually assumed to be of negligible importance in stellar systems which have lifetimes of only  $10^2 - 10^4$  dynamical times.

The qualitative nature of the diffusion seen in the present models has been discussed by a number of authors, especially Gerhard and collaborators (Gerhard & Binney 1985; Gerhard 1987), who showed that box orbits are destabilized by close passage to a central mass concentration. While the angle of deflection produced by even a  $1/r^2$  density cusp is generally small (Miralda-Escudé & Schwarzschild 1989), the dependence of this angle on pericenter distance is large, leading to a sensitive dependence of the orbital trajectory on initial conditions. A stochastic orbit in such a potential may look similar to a regular, box orbit for a limited time, but will eventually undergo a scattering event that moves the phase point to a different box orbit, etc. After a sufficiently long time, any such trajectory would be expected to uniformly fill the phase space region defined by all orbits that pass near the center at that energy (Gerhard & Binney 1985). The result is a time-averaged configuration-space density that is similar to, though rounder than, that of a typical box orbit.

Gerhard *et al.*’s numerical experiments in two spatial dimensions (see also Binney 1982a) show that this diffusion can be relatively fast, producing significant changes in the appearance of an orbit over just tens or hundreds of oscillations if the central mass concentration is sufficiently strong. The diffusion described by Gerhard and Binney can not be identified with Arnold diffusion, since Arnold diffusion does not exist in systems with only two degrees of freedom. Instead we associate it with the faster diffusion that occurs in a strongly chaotic part of phase space. We likewise assume that the orbital evolution seen in our three-dimensional models is best associated with this faster diffusion. Over much longer time scales, Arnold diffusion might lead to qualitatively different behavior for some orbits — we can say nothing useful about this based on our short integrations.

In our weak-cusp potential, inspection of the orbit plots reveals that most stochastic

trajectories do in fact mimic regular box orbits over 100 dynamical times: stochastic orbits of a given energy, but started from different initial points, retain distinctly different shapes over this limited period of time. In the strong-cusp potential, on the other hand, stochastic orbits quickly sample most of the configuration-space volume contained within the equipotential surface and attain a characteristic, roughly spherical shape that is distinctly different from that of a thin box orbit. Thus the stochastic orbits in the strong-cusp potential appear to diffuse over their allowed phase space volumes much more quickly than in the weak-cusp model – a result that is consistent with (though not strictly implied by) the generally larger Liapunov exponents of orbits in the strong-cusp model.

The central parts of many early-type galaxies are much older than 100 dynamical times. Using the parameters given in Table 4 of Lauer *et al.* (1995), we can compute approximate dynamical ages for “power-law” galaxies observed with HST. (We assume spherical symmetry, circular orbits and  $M/L = 10$  in solar units.) Defining a galactic lifetime as  $5 \times 10^9$  years, we find that stars in NGC 3115 would have completed  $10^3$  orbits at a radius of 540 pc ( $=0.20R_e$ );  $10^4$  orbits at 43 pc ( $0.016R_e$ ); and  $10^5$  orbits at 3.3 pc ( $1.3 \times 10^{-3}R_e$ ). In NGC 7332, we find dynamical ages of  $10^3$  at 450 pc ( $0.13R_e$ );  $10^4$  at 41 pc ( $0.012R_e$ ); and  $10^5$  at 3.6 pc ( $1.1 \times 10^{-3}R_e$ ). Both of these galaxies are luminous ( $M_B \approx -19.5$ ); lower-luminosity galaxies like M32 are typically denser and a larger fraction of the mass of such a galaxy would have undergone  $10^3$  or more orbits by now. Thus the behavior of a stochastic orbit during  $10^2$  dynamical times may not be a sufficient basis on which to build a model that will maintain its shape over the age of the universe.

We therefore investigated how the diffusion of the stochastic orbits affects their time-averaged density distributions over time scales longer than 100 periods. We integrated particular stochastic orbits for up to  $10^5 T_D$  in our two model potentials. To save computer time, the Liapunov exponents were not computed. Instead, the time-averaged occupation numbers in a grid of cells were recorded at 30, 100, 300, 1000, 3000,  $10^4$ ,  $3 \times 10^4$  and  $10^5$  orbital times. (The grid of cells was constructed as described in §5, except that the radial grid boundaries were equipotential surfaces, not equidensity surfaces.) In addition, we computed as a function of time a heuristic measure of the departure of the orbit from “ergodicity on the energy surface,” defined as follows.<sup>1</sup> In an imaginary potential characterized by no integrals of motion aside from the energy, every trajectory would be

---

<sup>1</sup> We follow the standard usage here, i.e. a “stochastic” or “chaotic” trajectory is one with non-zero Liapunov exponents, and an “ergodic” trajectory is one that uniformly fills some phase space volume – either the entire energy surface, or some allowed part of it – after infinite time. Ergodicity does not imply stochasticity; for instance, the motion of a regular orbit is ergodic over its invariant torus. Nor does stochasticity necessarily imply ergodicity, although motion in a fully stochastic phase space can sometimes be shown to be ergodic (Sinai 1976). Our usage differs from that of some authors, e.g. Goodman & Schwarzschild (1981) use the term “stochastic” to mean “filling the energy hypersurface.”

free to wander over every part of the energy surface  $E = E_0$ . Although the detailed trajectory of such an orbit is not possible to calculate, its asymptotic, time-averaged configuration space density would be

$$\rho_{erg}(\mathbf{x}) \propto \int \delta(E - E_0) d^3v \quad (17a)$$

$$\propto \int \delta(E - E_0) \sqrt{E - \Phi(\mathbf{x})} dE \quad (17b)$$

$$= C \sqrt{E_0 - \Phi(\mathbf{x})}, \quad \Phi(\mathbf{x}) \leq E_0; \quad (17c)$$

$$= 0, \quad \Phi(\mathbf{x}) \geq E_0.$$

Clearly we cannot expect any stochastic orbit in our model potentials to attain this density distribution, even after an infinite time, since no stochastic orbit can sample the regular parts of phase space. Nevertheless we might expect the time-averaged density of a stochastic orbit to approach  $\rho_{erg}$  fairly closely, particularly in models – like ours – where the fraction of phase space associated with stochastic orbits is large.

As a measure of the deviation of the time-averaged density of a stochastic orbit from this “fully ergodic” density, we defined

$$\Delta(t) = \int \left[ \frac{\rho_{erg}(\mathbf{x}) - \bar{\rho}(\mathbf{x}; t)}{\rho_{erg}(\mathbf{x})} \right]^2 \rho_{erg}(\mathbf{x}) d^3x, \quad (18a)$$

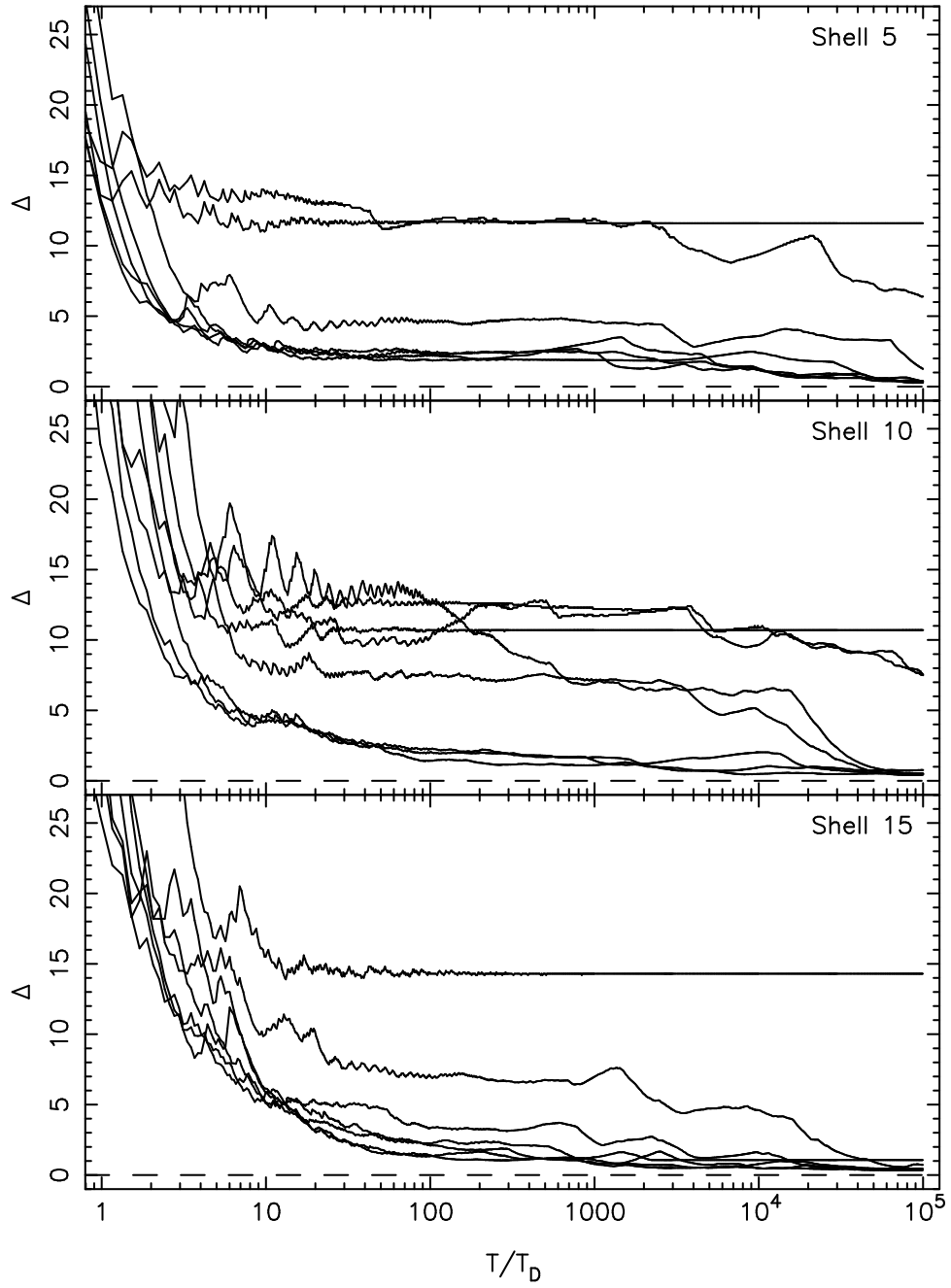
$$= \int \left[ \frac{\bar{\rho}(\mathbf{x}; t)}{\rho_{erg}(\mathbf{x})} \right] \bar{\rho}(\mathbf{x}; t) d^3x - 1 \quad (18b)$$

with  $\bar{\rho}(\mathbf{x}, t)$  the time-averaged density of the stochastic orbit at time  $t$ ; the second expression follows after assuming that  $\rho_{erg}$  and  $\bar{\rho}$  are normalized to unit total mass. Although  $\bar{\rho}(\mathbf{x}, t)$  is not a well-defined quantity for a single trajectory, we can compute a coarse-grained approximation by recording passages of the trajectory through a grid of cells; for our purposes, a natural set of cells are the ones just described. We then have:

$$\Delta(t) \approx \sum_{cells} \frac{\bar{m}^2(t)}{m_{erg}} - 1, \quad (18c)$$

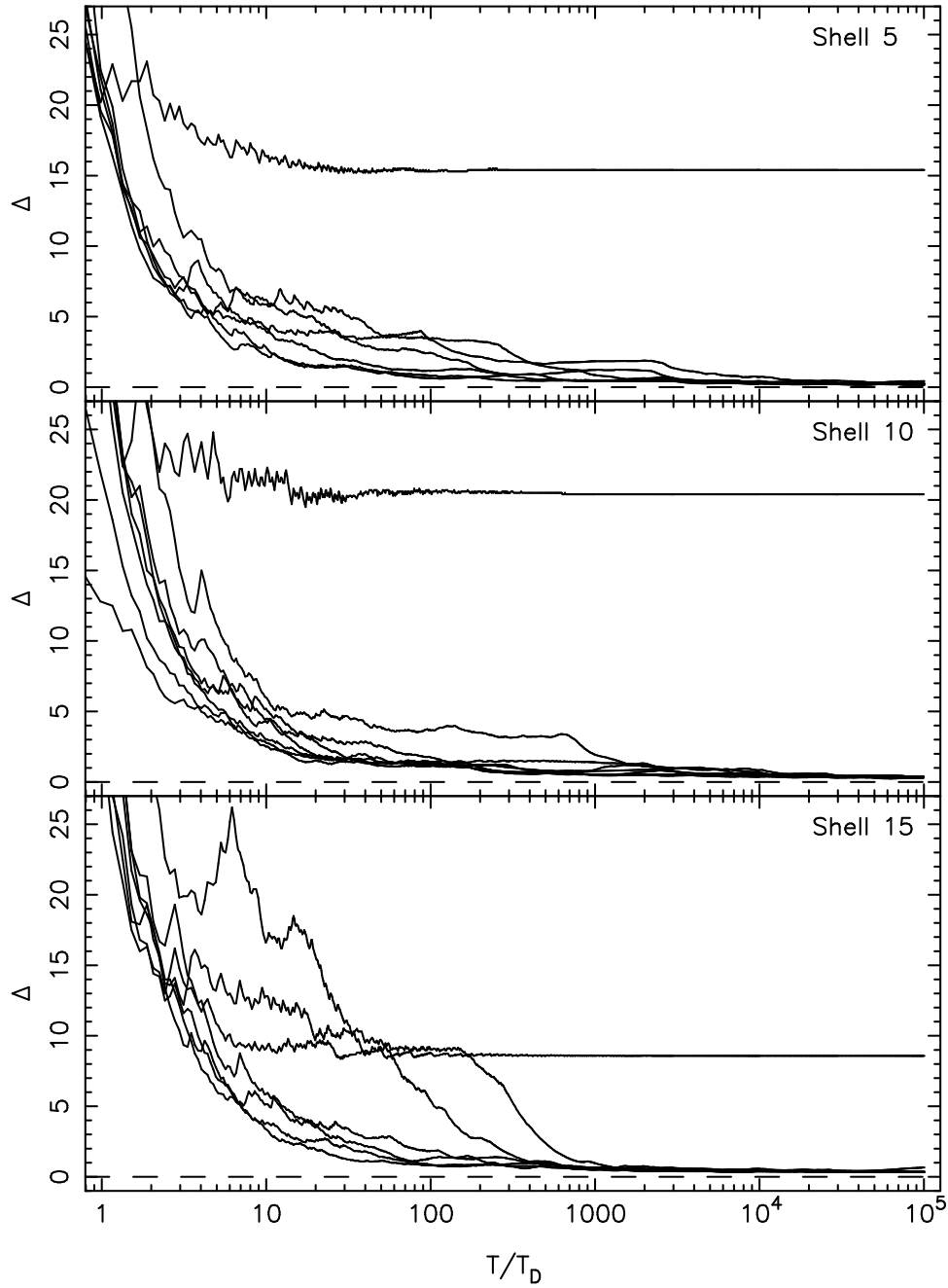
with  $\bar{m}$  the time-averaged mass of the orbit in one grid cell, and  $m_{erg}$  the mass of the “fully ergodic” orbit in that cell. The parameter  $\Delta(t)$  is zero if and only if the stochastic orbit has a time-averaged density that is everywhere identical to that of the “fully ergodic” orbit of the same energy. A value of  $\Delta = p^2$  indicates that the rms deviation of the cell mass from that of the “fully ergodic” orbit is  $p$ .





8a. Approach to ergodicity for stochastic orbits in the weak-cusp models.

Figure



Figure

8b. Approach to ergodicity for stochastic orbits in the strong-cusp models.

Figure 8 shows the evolution of  $\Delta(t)$  for a set of stochastic orbits. In each of the two model potentials, stochastic orbits from the stationary start space were integrated at three energies corresponding to shells 5, 10 and 15. These orbits were chosen to have

Liapunov exponents – computed over  $100 T_D$  – spanning the observed range for orbits at that energy. The evolution of  $\Delta(t)$  for one regular orbit at each energy is shown for comparison.

Figure 8 illustrates the above-mentioned difference between the stochastic orbits in the two potentials. In the strong-cusp potential, all of the stochastic orbits evolve rapidly toward a well-defined, time-averaged state that is similar to that of the fully ergodic orbit of the same energy, and very different from that of a typical regular orbit. Even after  $\sim 10^2$  oscillations, most stochastic orbits have spatial distributions that are closer to each other than they are to a typical regular orbit – consistent with the conclusions reached on the basis of the orbital plots. By  $10^3$  or  $10^4$  dynamical times, the time-averaged densities of the stochastic orbits are almost indistinguishable from one another, though they remain distinctly different from that of the fully ergodic orbit, with  $\Delta \approx 0.3 \pm 0.05$ . Thereafter, the time-averaged densities remain nearly constant.

By contrast, the stochastic orbits in the weak-cusp potential are generally slower to fill their allowed phase-space volumes, and some apparently never do. After  $10^2$  orbital times, there is as much spread in the  $\Delta$  values among the stochastic orbits as between stochastic and regular orbits; and even after  $10^4$  or  $10^5$  dynamical times the time-averaged densities of some of the stochastic orbits are showing little tendency to evolve toward a steady state (although a few appear to be nearly as “ergodic” as the orbits in the strong-cusp potential). A typical stochastic orbit in this potential appears to remain confined to a restricted region of phase space over hundreds or thousands of oscillations at least; thus many of the stochastic orbits in this model can mimic regular orbits for periods of time that are comparable to the age of the universe. This result is consistent with that of other workers who found that the stochastic orbits in nearly-integrable potentials are far from ergodic over the energy surface on short time scales (e.g. Goodman & Schwarzschild 1981).

Figure 8 suggests that – in at least the strong-cusp model – we can define a single time-averaged density distribution that represents every stochastic orbit at a given energy. This time-averaged density is illustrated in Figure 9 for shell 10; the cell occupation numbers are averages from six stochastic orbits, each integrated for  $10^5$  dynamical times. (Each individual stochastic orbit produced a time-averaged distribution that differed only slightly from this average.) Also shown for comparison is the density distribution of the “fully ergodic” orbit, equation (17), of the same energy, as well as a “boxlet” from the 4:5:7 resonant family. The stochastic and fully ergodic density distributions are similar in the sense that all cells lying within the equipotential surface are occupied. However the stochastic orbit spends proportionately more time near that surface. In addition, the stochastic orbit is more highly flattened: the occupation numbers of cells near the  $x$ -axis are relatively higher than those of the fully ergodic orbit when compared to cells near the  $y$ - and  $z$ -axes. This flattening of the stochastic orbit can be understood in one of two ways. On the one hand, the stochastic trajectory may be seen as a superposition of regular box orbits, as described by Gerhard & Binney (1985). Since box orbits are

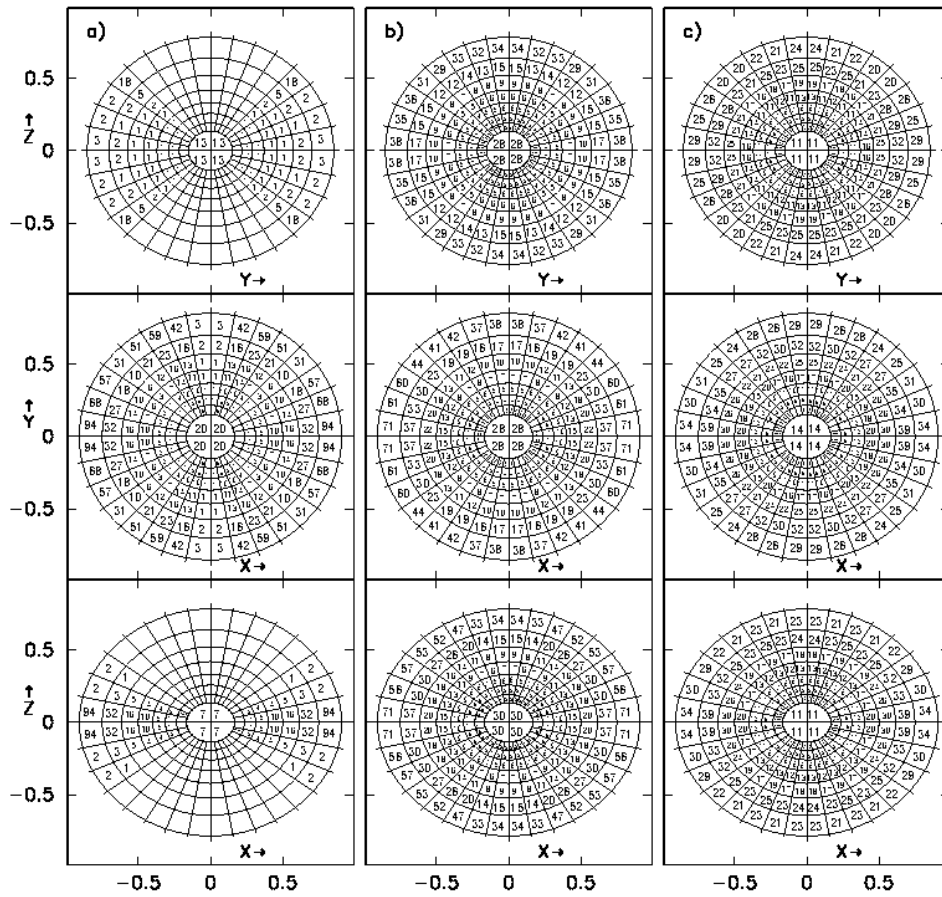


Figure 9. Three cross sections through a regular orbit (a), a time-averaged stochastic orbit (b) and a “fully ergodic orbit” (c) from shell 10 in the strong-cusp model. The number in each cell represents the fraction of time (scale arbitrary) which the orbit spends in the cell (numbers were replaced by dots in some of the inner shells). Cells without numbers are not entered by the orbit.

primarily aligned along the  $x$ -axis, it is not surprising that the time-averaged trajectory of a stochastic orbit shows a similar elongation. On the other hand, we can think of the stochastic trajectory as similar to the fully ergodic trajectory minus those parts of phase space that are regular. The regular parts of phase space consist mostly of tube orbits, and orbits from the tube families tend to enhance the density more parallel to one of the shorter two axes than parallel to the longer two axes. Excluding these parts of phase space from the regions visited by the stochastic trajectory would again imply a time-averaged density that is elongated along the long axis.

These results suggest that the stochastic orbits in models with strong cusps can explore their full phase space volumes over time scales of order  $10^2 - 10^3$  dynamical times. Thus – at least in the inner regions of a model where the orbital times, scaled to a real galaxy, would fall below  $\sim 10^{-3}$  of the age of the universe – we must replace all the stochastic orbits of a given energy by a single, time-averaged orbit that represents a uniform density of stars within the stochastic part of phase space.

In models with a weak cusp, where diffusion time scales are longer, one might be justified in assigning arbitrary occupation numbers to “different” stochastic orbits of the same energy, each integrated for a finite time. However Figure 8 shows that many stochastic orbits even in the weak-cusp potential behave nearly ergodically over modest time scales, and a self-consistent solution that includes distinguishable stochastic orbits would therefore not represent a true equilibrium. Furthermore one can imagine physical processes that might enhance the diffusion rate above what is seen in Figure 8. We return to these questions in §5.

We note that the estimation of phase-space filling rates via time-averaging is not strictly justified, since nature is more concerned with the evolution of ensembles of orbits than with time-averages of individual orbits. For instance, a regular orbit fills its torus in a time-averaged sense within a few tens of crossing times, as shown here, but an ensemble of points on a given torus *never* reaches an equilibrium distribution – the ensemble simply translates, unchanged, around the torus. The physically more interesting timescale is the “mixing” time, i.e. the time required for an initially non-random distribution of stars in phase space to mix into a time-invariant state. Regular orbits, unlike chaotic orbits, do not mix, at least in a fixed potential, and it is unclear how to define mixing rates for these orbits in a manner that allows a meaningful comparison with chaotic orbits. A fuller discussion of these issues may be found in Merritt (1996).

#### 4.3. Comparison with Earlier Work

The results described in this section are surprising in at least one respect. Earlier studies of the dependence of stochasticity on cusp strength (e.g. Gerhard & Binney 1985; Gerhard 1987) suggested that while stochasticity would be important in a triaxial model with a strong cusp,  $\rho \propto 1/r^2$  or steeper, the orbital population of a model with a cusp as weak as  $\rho \propto r^{-1}$  would be essentially similar to that of a fully regular model. These studies were mostly based on surfaces of section describing the two-degrees-of-freedom motion in

one of the principal planes. In the present study (based admittedly on a single choice for the axis ratios of the figure) we reach a very different conclusion: the fraction of stochastic orbits is quite large even for weak cusps. How can this discrepancy be understood?

Discussions with O. Gerhard and D. Pfenniger led to the following insights. Surfaces of section based on motion in the principal planes can be misleading about the full, three-dimensional motion. This is because, first, periodic orbits which generate families of regular orbits in the principal planes are often unstable to perturbations out of the plane; second, there are families of orbits that exist entirely outside of the principal planes and so make no appearance on the surfaces of section; and third, the time scale required for an orbit to manifest its stochasticity may be rather longer than the typical integration time used in constructing a surface of section.

We constructed surfaces of section in the three principal planes of our models and found that the vertical instability of the planar periodic orbits is the most important of these three factors. Only the  $x - z$  bananas, among all the low-order planar periodic orbits, is stable at most energies to vertical perturbations in our models (Tables 3 and 5). Thus the surfaces of section in the  $x - y$  and  $y - z$  planes show large regions of regular motion associated with the banana, fish etc. orbits, while in fact this regularity is destroyed once the motion is perturbed out of the plane. Indeed, based on the surfaces of section, it is the  $x - z$  plane that contains the *greatest* amount of stochastic motion (generated by the unstable  $x$  and  $z$ -axial orbits), while in fact the 3-D motion in the vicinity of this plane is much *more* regular than around the other two due to the vertical stability of the  $x - z$  bananas.

## 5. CONSTRUCTION OF SELF-CONSISTENT MODELS

Self-consistent solutions were constructed in the usual manner (Schwarzschild 1979). The fraction of time spent by each orbit in a grid of cells was recorded, then a linear superposition of orbits was sought, with non-negative occupation numbers, that reproduced the known mass of the model in each cell.

The grid of cells was defined as follows. As described above, the models were divided by 20 ellipsoidal shells into 21 sections of equal mass. Each octant of each section was then divided into 48 facets, in the following manner. The octants were first divided into three sectors by the planes  $z = cx/a$ ,  $y = bx/z$  and  $z = cy/b$ . Then each sector was divided into 16 facets by a set of six planes. In the case of sector one, which contained the  $x$ -axis, these planes were defined by  $ay/bx = 1/5, 2/5, 2/3$  and  $az/cx = 1/5, 2/5, 2/3$ . The facets in the other two sectors were defined in a symmetric way. This grid cell structure has the advantage that the mass which the model places in each cell is roughly the same, and furthermore these masses are precisely independent of the model axis ratios (although they still depend on the density profile, as specified by  $\gamma$ ).

The problem to be solved is a constrained optimization problem. The quantity to be optimized (minimized) is the discrepancy between the model cell masses, and the cell

masses generated by some linear combination of the orbits; the constraints include, among other possible things, the non-negativity of the orbit occupation numbers.

Various criteria have been adopted in the past for deciding when a combination of orbits comes “close enough” to reproducing the model cell masses. Schwarzschild (1979) originally required his solutions to reproduce each of the cell masses to within machine precision. More recently (Schwarzschild 1993), he has required only that the maximum error in one grid cell not exceed 1%.

Clearly a requirement that the model densities be reproduced to within machine precision is overly stringent given the other approximations that are made in the construction of the model (finite integration times, discrete grids, etc.) Furthermore the problem that we are solving is ill-conditioned (O’Sullivan 1986) in the sense that any attempt to find a numerically exact solution of the discretized equations will generate large-amplitude fluctuations in the weights from orbit to orbit. Such an unsmooth solution is not necessarily a relevant model for a real galaxy; a better goal would be to find a solution that is smooth in phase space but which (as a consequence of the smoothness constraint) might only reproduce the cell masses approximately. A further argument against requiring exact self-consistency is that failure to reproduce the cell masses exactly may only mean that the orbit library is not sufficiently dense to cover the phase space in a fully representative way.

We attempted to demonstrate self-consistency by giving larger and larger subsets of our orbit libraries to the optimization routine, and observing how the average error in the cell masses varied with orbit number. One might expect that – if a self-consistent solution exists – the error in the cell masses would decrease rapidly once the number of orbits in the solution exceeded the number of grid cells, roughly  $10^3$ . On the other hand, a more gradual decrease of error with orbit number would suggest the nonexistence of a self-consistent solution. (Of course, our scheme does not rule out the possibility of reproducing the cell masses exactly and in fact this sometimes occurred in practice.) We then attempted to construct smooth solutions, to verify that the self-consistency was not an artifact of the discretization.

This scheme has the advantage of permitting a meaningful comparison between solutions obtained using different subsets of orbits, e.g. all orbits, regular orbits only, etc. The disadvantage, of course, is that there may be cases where the error falls neither so slowly nor so rapidly with number of orbits that one can clearly decide whether a self-consistent solution exists.

We chose to minimize the mean square deviation in the cell masses,

$$\chi^2 = \frac{1}{N} \sum_{l=1}^N \left[ D_l - \sum_{i=1}^M C_i B_{il} \right]^2, \quad (19)$$

where  $C_i$  is the number of stars on orbit  $i$ ,  $1 \leq i \leq M$ ;  $B_{il}$  is the mass which the  $i$ th orbit places in the  $l$ th cell; and  $D_l$  is the mass which the model places in the  $l$ th cell. Self-

consistency was not sought in the outermost shell of grid cells, since few orbits supplied densities in these cells. Thus  $N = 912$  is the number of grid cells in the model excluding those in the outer shell.

The basic set of constraints was

$$C_i \geq 0, \quad (20)$$

i.e. nonnegative orbit weights. Other constraints are discussed below.

The constrained optimization problem represented by equations (19) and (20) is an example of quadratic programming. We used the NAG routine E04NCF to carry out the optimization. A solution using the full set of orbits required about six hours on a DEC Alpha 3000/700 computer.

### 5.1. *Quasi-Equilibrium Solutions*

Not all solutions to the self-consistency equations presented above represent fully stationary galaxy models. The orbits in our libraries were integrated for only 100 dynamical times, and the stochastic orbits do not reach their invariant distributions in such a short time. We can nevertheless attempt to construct “quasi-equilibrium” solutions in which we treat the stochastic and regular orbits in the same way, allowing each stochastic orbit to have an arbitrary occupation number. Such models would, if allowed to evolve, presumably change shape near the center as the stochastic orbits gradually filled phase space in a time-independent way. Nevertheless they provide a useful starting point for considering more fully stationary models.

Figure 10 shows the departure from self-consistency, as a function of the number of orbits supplied to the optimization routine, for the two mass models. Orbits were chosen by selecting every 10th, every 5th, etc. orbit from the complete libraries of 6840 orbits. The departure from self-consistency was defined as

$$\delta = \frac{\sqrt{\chi^2}}{\text{average mass/cell}},$$

i.e. the percentage, rms deviation in the cell masses. Figure 10 shows that both mass models admit quasi-stationary solutions to the self-consistency equations. The weak-cusp model yields  $\delta = 0$  when the number of orbits exceeds  $\sim 3000$ , while the strong-cusp model shows a slight departure from numerical self-consistency,  $\delta \approx 2 \times 10^{-4}$ , even when the full set of orbits is used. However Figure 10 strongly suggests that including a slightly larger number of orbits in the strong-cusp solution would give exact self-consistency for this mass model as well.



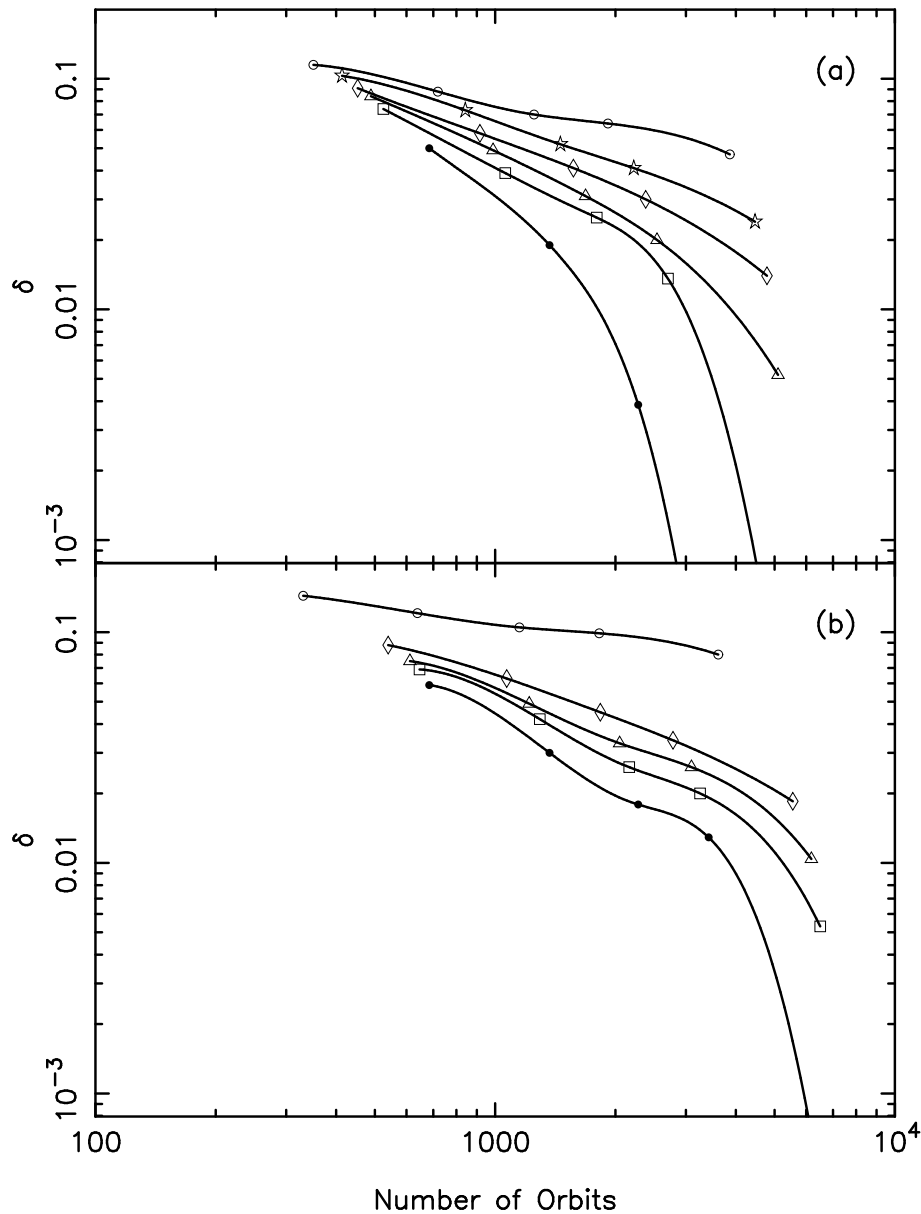


Figure 10. Departure from self-consistency ( $\delta$ ) as a function of number of orbits supplied to the optimization routine, for the weak-cusp (a) and strong-cusp (b) models.  $\circ$ : regular orbits only;  $\bullet$ : all orbits. The intermediate curves in (a) represent solutions in which the stochastic orbits were included only in shells above 10 ( $\square$ ), 12 ( $\triangle$ ), 14 ( $\diamond$ ), and 16 ( $\star$ ). In (b), the intermediate curves represent solutions in which the stochastic orbits were included only in shells above 2 ( $\square$ ), 4 ( $\triangle$ ) and 8 ( $\diamond$ ).

One (rather artificial) way to construct fully stationary solutions is to supply only the

regular orbits to the optimization routine. Excluding all stochastic orbits leaves 3864 and 3616 regular orbits, respectively, in the weak- and strong-cusp orbit libraries. Figure 10 shows that the regular orbits alone can reproduce the model cell densities with an accuracy of only  $\delta \approx 5\%$  in the weak-cusp model and  $\sim 8\%$  in the strong-cusp model; furthermore the weak dependence of  $\delta$  on orbit number does not give confidence that a larger number of orbits would greatly reduce the error. We conclude that the regular orbits – the tubes and boxlets – do not provide a wide enough variety of shapes to reproduce the triaxial figure in either mass model. However the regular orbits go farther toward reproducing the model density in the weak-cusp case, presumably because of the greater variety of boxlet families in this potential (Fig. 4).

Since the diffusion time scale for stochastic orbits is a strong function of their energy, one might hope to construct a nearly stationary model by simply excluding the stochastic orbits with energies below some threshold. The resulting self-consistent solution, if it exists, would depart only negligibly from equilibrium at radii less than the typical radius of the most bound stochastic orbits included.

Figure 10 demonstrates that such “nearly equilibrium” solutions can in fact be found, at least for the weak-cusp model. Removing all of the stochastic orbits inside shell 10 — roughly the inner half-mass radius — does not destroy the self-consistency of this solution. Since the diffusion time scale for stochastic orbits outside of the half-mass radius of a galaxy is likely to exceed  $10^{10}$  years (§4), we conclude that a galaxy constructed in this way would be effectively stationary for a Hubble time.

In the case of the strong-cusp model, however, the deviation from exact self-consistency increases rapidly as one excludes stochastic orbits from larger and larger regions near the center. Figure 10 suggests that only the stochastic orbits inside shell 1 or 2 can be excluded without destroying self-consistency.

Schwarzschild (1993) found that he could achieve nearly exact self-consistency in a scale-free,  $\rho \propto r^{-2}$  triaxial model, with  $c/a = T = 1/2$ , using only the regular orbits. Schwarzschild’s model can be seen as an approximate representation of the central parts of our strong-cusp model where the density also varies as  $\sim r^{-2}$ . Our new result is consistent with Schwarzschild’s, but suggests that self-consistency using just the regular orbits becomes more difficult as one includes parts of the model that are not scale-free. One contributing factor is that the  $x-z$  “banana” orbits – which were found to contribute about 80% of the mass not associated with tube orbits in these fully-regular solutions – become more sharply bent at large energies, and thus less able to maintain the strong flattening of these models at large radii. Regular orbits alone might therefore have sufficed if our mass model had been chosen to be more nearly round. In addition, Figure 6 shows that – while the fraction of regular orbits is not a strong function of energy in the strong-cusp model – the regular orbits at high energies belong primarily to just one family, the  $x-z$  bananas. At low energies, in the scale-free part of the potential, a wider variety of regular orbit families are available for building a model.

### 5.2. Fully-Mixed Solutions

The experiments just described demonstrate that one can construct nearly-stationary triaxial models of galaxies with weak cusps by including stochastic orbits only at high energies. But nature would almost certainly not build galaxies in this way, since it has no mechanism for selectively placing stars on regular or stochastic orbits and would therefore tend to populate these two parts of phase space in rough proportion to their volumes. Here we explore self-consistent solutions in which the stochastic parts of phase space are strongly populated, but (unlike in the solutions described above) in an approximately time-independent manner.

We begin by noting that Jeans's theorem can be generalized to include the (generic) case of a galaxy in which not all of the orbits are regular. The first step is to divide phase space into regular and stochastic regions. In the regular parts of phase space, orbits are characterized by two isolating integrals in addition to the energy, and the Jeans theorem in its usual form is valid: the steady-state distribution function  $f_R$  – which must be single-valued and constant along trajectories – can depend on the phase space coordinates only through the isolating integrals of motion,  $f_R = f_R(E, I_2, I_3)$ . (Note that the integrals  $I_2$  and  $I_3$  are now local, not global, invariants and so their definitions will change from one regular region to another.) In the stochastic parts of phase space, which are interconnected through the Arnold web, strict constancy of  $f$  along trajectories requires that the phase space density have a single value throughout the entire stochastic region at every given energy; thus  $f_S = f_S(E)$ . The penalty for violating this condition will only be severe if the stochastic orbits undergo significant diffusion on time scales of interest, however.<sup>2</sup>

A steady-state galaxy will therefore have a distribution function of the form

$$f = \begin{cases} f_R(E, I_2, I_3) & \text{(regular phase space)} \\ f_S(E) & \text{(stochastic phase space)} \end{cases} \quad (21)$$

where it is understood that the integrals  $I_2$  and  $I_3$  are local, not global, invariants of the motion. We will refer to a model that is described by equation (21) as “fully mixed”.

It was shown above that the diffusion time for stochastic orbits in the strong-cusp potential was relatively short, of order  $10^2 - 10^3$  dynamical times. This result suggests that fully-mixed models might be relevant to at least the central parts of real galaxies with strong cusps. But even when modelling the outer parts of a galaxy, or the inner parts

---

<sup>2</sup> Binney (1982b) expressed the view that Jeans's theorem applies only to completely integrable systems. His central points, with which we agree, are that ergodicity can only be rigorously proved for regular orbits, and stochastic orbits may take a very long time to uniformly fill their allowed phase-space regions. However Liouville's theorem guarantees that an *initially* uniform distribution of points in any bounded phase-space region will remain uniform forever, and this is true whether the phase-space region is regular or stochastic; the ergodicity of individual orbits is irrelevant.

of a galaxy with a weak cusp, where diffusion time scales are relatively long, it is still interesting and appropriate to construct fully-mixed models, for the following reasons.

1. If a fully-mixed solution corresponding to a given mass model can not be found, then any galaxy with the same mass distribution must be slowly evolving due to the continued mixing of its stochastic orbits. The non-existence of fully-mixed models thus has interesting consequences for the dynamical states of real galaxies.

2. A number of physical processes can be imagined that would increase the diffusion rate of stochastic orbits above what has been calculated here; and there is no obvious mechanism that would decrease it. For instance, many elliptical galaxies contain deviations from ellipsoidal symmetry in the surface brightness at the  $\sim 1\%$  level, e.g. “boxy” or “disky” isophotes (e.g. Nieto & Bender 1989). These distortions – to the extent that they are reflected in the gravitational potential – might be expected to enhance stochasticity above what is observed in perfectly ellipsoidal models like ours (Udry & Pfenniger 1988). Star-star interactions in a dense nucleus would help to scatter trajectories in phase space by providing random, time-dependent force perturbations (e.g. Goodman & Schwarzschild 1981). Any additional central mass concentration, such as a massive black hole or dense stellar nucleus, would produce occasional, large-angle deflections in orbits passing near the center (Gerhard & Binney 1985). Tidal forces from nearby galaxies might also provide a time-dependent perturbing force for stars on high-energy orbits. These extra sources of diffusion might be of rather different importance in different galaxies, but each would act to enhance the mixing of stochastic orbits above that observed in simpler models.

3. Rapid and chaotic changes in the gravitational potential during the formation of a galaxy are thought to redistribute stars in phase space on a time scale that is of order the collapse time (Lynden-Bell 1967). These fluctuations act equally on stars whether or not they lie in regular parts of phase space (or will lie in such regions, after the potential reaches a steady state); their net result is to generate a nearly uniform population of stars on constant energy surfaces. We might therefore expect some galaxies to *begin* their lives in highly mixed states. The strength of this argument depends on the efficiency of violent relaxation and it is likely to be only more or less correct in any particular galaxy. Nevertheless one could take the view that the “most probable” model for a galaxy is one in which the stochastic parts of phase space are uniformly populated.

One way to construct numerical approximations to fully-mixed models would be to carry out very extended integrations of orbits in the stochastic parts of phase space at every energy and record their time-averaged densities. Such experiments were described in §3. If the time integrations were sufficiently long, then every such time-averaged trajectory would approximate a uniform population of the stochastic part of phase space and could be treated like a regular orbit in the model construction – with the important difference that only *one* such orbit would be available at each energy.

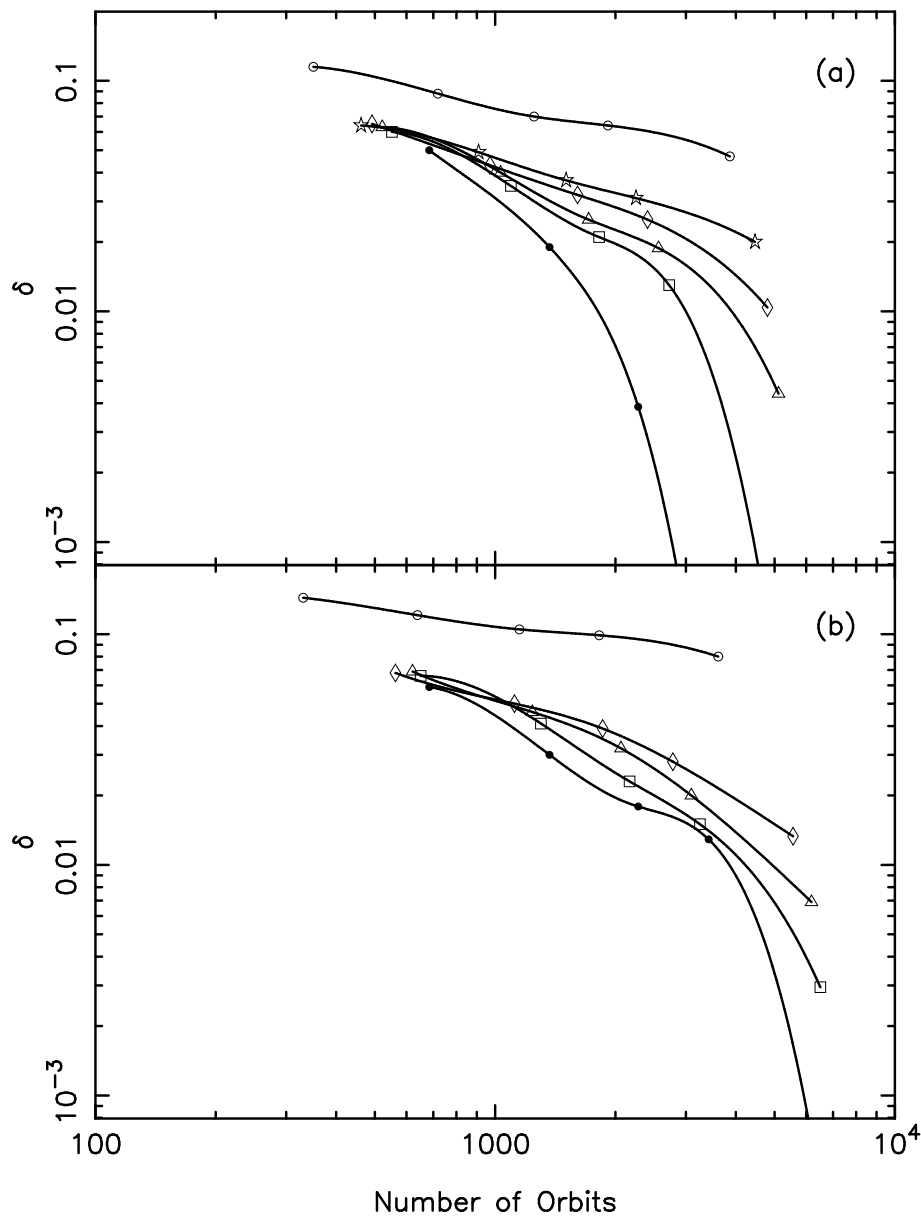


Figure 11. Departure from self-consistency ( $\delta$ ) as a function of number of orbits supplied to the optimization routine, for solutions in which the stochastic orbits are “fully-mixed” below some energy. (a) Weak cusp; (b) Strong cusp. The intermediate curves in (a) represent solutions in which the stochastic orbits were forced to be fully-mixed in shells below and including 10 ( $\square$ ), 12 ( $\triangle$ ), 14 ( $\diamond$ ), and 16 ( $\star$ ). In (b), the intermediate curves represent solutions in which the stochastic orbits were fully mixed in shells below and including 2 ( $\square$ ), 4 ( $\triangle$ ) and 8 ( $\diamond$ ).

Following a suggestion of Ya. G. Sinai, we chose instead to approximate these time-

averaged densities by simply arithmetically averaging the densities of the  $\sim 100$  stochastic orbits at each energy in our orbit libraries, each already computed for the standard 100 dynamical times. In other words, we replaced a time average by an ensemble average – a generally more efficient way to proceed, particularly in the case of the weak-cusp model where the diffusion times are long. We verified that these ensemble averages approximated closely the direct time averages presented for a few stochastic orbits in §3.

One way to implement Prof. Sinai’s suggestion is to simply include the additional constraints

$$C_j = C_k \tag{22}$$

into the quadratic programming routine, where  $j$  and  $k$  are understood to refer to every pair of stochastic orbits of the same energy. An equivalent, and computationally more efficient, approach is to replace the stochastic orbits in the orbit libraries by their arithmetic average at each energy before carrying out the optimization. The latter approach reduces the number of orbits that are supplied to the quadratic programming routine and so increases its speed; we followed it in the experiments described below.

The additional constraints represented by equation (22) will make it more difficult to find a self-consistent solution than if each stochastic orbit were allowed to have its own weight, as in the quasi-equilibrium solutions described above. On the other hand, the time-averaged stochastic orbits (Fig. 9) are elongated in approximately the same sense as the model figure, and including them in the orbit library gives the optimization routine slightly more flexibility – in the form of just a single extra “orbit” at each energy – than it would have if only the regular orbits were included.

As Figure 11 shows, this slight additional freedom allows the quadratic programming routine to reduce the residuals somewhat compared to the solutions which exclude the stochastic orbits completely below some energy. For instance, in the strong-cusp model,  $\delta$  drops by a factor of  $\sim 2$  when the fully-mixed stochastic orbits are added to the regular orbits in the innermost shells. Less improvement is seen in the weak-cusp solutions — here, the regular orbits provide a larger fraction of the mass near the center.

Although the fully-mixed stochastic orbits are not a great asset from the point of view of constructing a self-consistent model, are they a serious liability? In other words, could a galaxy place a large number of stars on such orbits without destroying the self-consistency? To investigate this question, we attempted solutions in which the weights assigned to the time-averaged stochastic orbits were increased as far as possible without violating self-consistency. Figure 12 shows one example for each mass model. The weak-cusp solution shown there, which is completely self consistent ( $\delta = 0$ ), was constructed by maximizing the numbers of stars on fully-mixed stochastic orbits from shells 1 through 6; stochastic orbits with larger energies were allowed to have arbitrary occupation numbers. The fully-mixed stochastic orbits carry approximately one-third of the mass near the model center, while at larger energies, stochastic orbits – no longer fully mixed – dominate. The “boxlets” are important only at low energies, where they likewise contribute about

one-third of the mass; at high energies their contribution is negligible. Overall, stochastic orbits contribute 45%, and boxlets only 11%, of the total mass in this solution.

The strong-cusp solution in Figure 12 contains fully-mixed stochastic orbits at only the two lowest energies; we find  $\delta = 3.3 \times 10^{-3}$ , nearly self-consistent. Once again the stochastic orbits are dominant at almost every energy, contributing 60% of the total mass; boxlets carry only 4%.

We conclude that a substantial population of stars distributed uniformly throughout stochastic phase space at low energies is consistent with self-consistency in our weak-cusp model. In the strong-cusp model, only the cusp itself can be so populated without violating self-consistency.

### 5.3. Smooth Solutions

One disadvantage of an orbit-based approach to model building is that the solutions are extremely unsmooth. One source of this lack of smoothness is the discrete way in which phase space is sampled. But even more important is the inherent ill-conditioning of the self-consistency problem. A single orbit, which represents a delta-function in integral space, covers a finite region in configuration space. Deriving the integral-space density from the configuration space density is therefore in the nature of a deconvolution problem, and deconvolution has the property of amplifying errors or incompleteness in the “data” (in our case, the masses which the models place in the cells). Even a highly noisy set of orbital weights can generate a smooth configuration space density, and there are many more noisy solutions than smooth ones. This effect actually becomes *worse* as the number of orbits is increased, since a fine grid is better able than a coarse grid to represent high-frequency fluctuations (Phillips 1962). In the absence of the non-negativity constraints, we would therefore expect our solutions to exhibit wildly variable occupation numbers from orbit to orbit, with many of the occupation numbers negative. Even enforcing positivity should only reduce, not eliminate, these fluctuations by “clipping” the negative occupation numbers at zero. Indeed, many or most of the orbital weights in the solutions described above were found to be zero, even when the number of orbits supplied to the optimization routine was smaller than the number of grid cells in which the mass was specified.<sup>3</sup>

Since our mass model is completely smooth, we might reasonably require the phase-space density of our self-consistent solutions to be smooth as well. An unsmooth solution could be acceptable, but only if it can be shown to have average properties that are close to those of a smooth solution. If, however, imposing smoothness on a numerical solution

---

<sup>3</sup> Schwarzschild (1993) notes that his Richardson-Lucy algorithm often required a very large number of iterations,  $\sim 4 \times 10^4$ , before reaching approximate self-consistency. This is a possible indication that his solutions were extremely unsmooth, since Lucy’s method always iterates toward an increasingly noisy solution. It may also imply that self-consistency was inconsistent with smoothness for his models, since a smooth solution would presumably have been reached more quickly if it had existed.

causes it to depart strongly from self-consistency, one would conclude that no solution continuous in the phase-space density exists, and that the apparent self-consistency is a numerical artifact associated with the discretization. It is primarily to address this concern that we now consider a modified algorithm that generates smooth solutions.

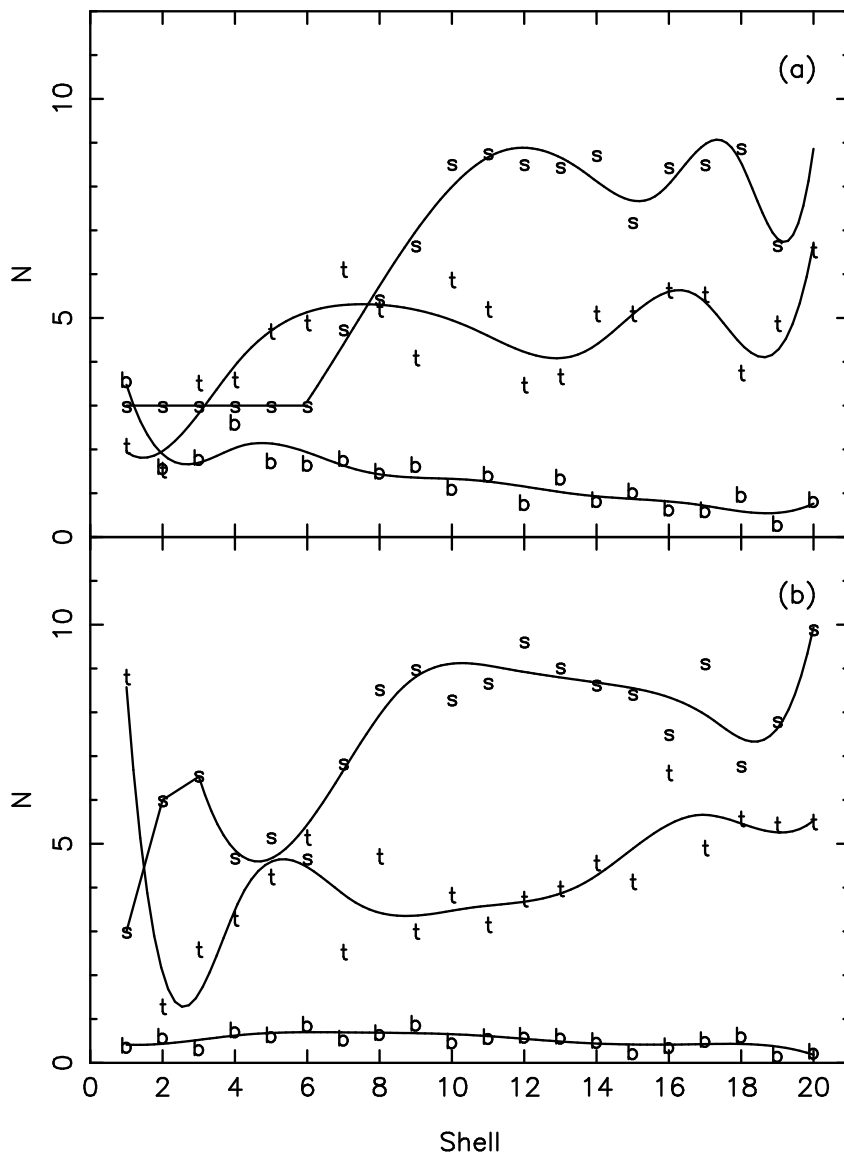


Figure 12. Orbital

content as a function of shell number for a weak-cusp (a) and strong-cusp (b) solution. In (a), the solution is fully mixed in shells below and including 6; in (b), the solution is fully mixed in shells 1 and 2. The symbols  $s$ ,  $t$  and  $b$  denote stochastic, tube and boxlet orbits respectively. The vertical axis is the number of stars from the indicated shell on orbits of the three types (arbitrary normalization).



A proper prescription for smoothness in our case is that the density be continuous in action space. This is a difficult prescription to apply, since our phase space is very complex and we have not computed the actions associated with even the regular orbits. Instead we will require simply that the orbital weights vary more-or-less smoothly over our initial condition grids: that is, that

$$C_j \approx C_k, \quad (23)$$

where  $j$  and  $k$  represent two orbits with adjacent initial conditions. Following Phillips (1962) and Tikhonov (1963), the large number of constraints implied by equation (23) can be imposed by adding a single term, a “penalty function,” to the optimization functional of equation (19). The quantity to be optimized becomes

$$\chi^2 = \frac{1}{N} \sum_{l=1}^N \left[ D_l - \sum_{i=1}^M C_i B_{il} \right]^2 + \alpha \sum_{i=1}^M g(C_i) \quad (24)$$

subject to constraint (20) (nonnegative  $C_i$ ’s). We chose  $g(C_i)$  to have the simple form

$$g(C_i) = C_i^2. \quad (25)$$

This is “zeroth-order regularization” (e.g. Miller 1974), and has the effect of filtering fluctuations on “scales” shorter than some maximum value determined by the smoothing parameter  $\alpha$ . (One might interpret (25) as defining a kind of entropy (Tremaine, Hénon & Lynden-Bell 1986; Richstone & Tremaine 1988). We do not encourage that interpretation, preferring instead to think of our penalty function as an *ad hoc* numerical device. See Jaynes (1984) and Binney (1987) for a similar point of view.) Our goal is to show that there is some choice for  $\alpha$  that reproduces approximately the fully-mixed solutions described above, while at the same time keeping the orbital weights from varying too strongly from grid point to grid point.

Figure 13 shows how the deviation from self-consistency, as measured by  $\delta$ , depends on the variance in the orbital weights for the two models displayed in Figure 12. We measured the variance via

$$\text{VAR}^2(\alpha) = \frac{\sum^M (C_i - \overline{C_i})^2}{M \overline{C_i}^2} \quad (26)$$

with  $M$  the number of orbits in the solution and  $\overline{C_i}$  the arithmetic average of the orbital weights. Because of computer limitations we computed these smooth solutions using only one-half of the orbits in our libraries; the  $\delta$  values are correspondingly larger than if all the orbits had been used. Figure 13 shows exactly the hoped-for behavior: as the solutions are gradually made smoother (i.e.  $\alpha$  is increased above zero), the departure from self-consistency remains almost constant and small. Only when the smoothing parameter  $\alpha$

is increased to the point that the variance becomes unrealistically small ( $\lesssim 1$ ) does  $\delta$  become unacceptably large.

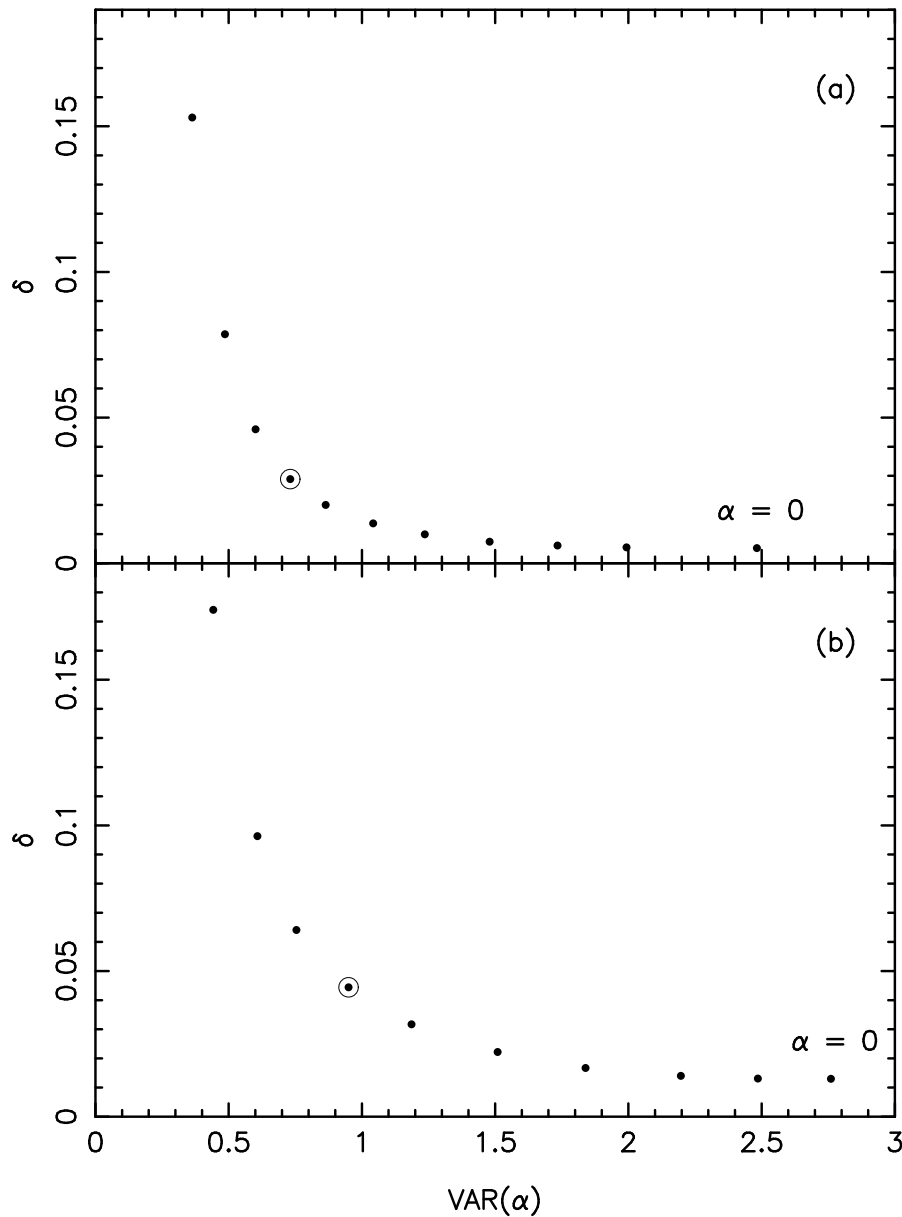


Figure 13. Deviation from self-consistency ( $\delta$ ) as a function of variance in the orbital weights for the two models illustrated in Figure 12. (a) Weak cusp; (b) strong cusp. The circled dots are the solutions represented in detail in Fig. 14.

Figure 14 displays the orbital fractions as a function of shell number for two of these smooth solutions. The orbital fractions are very similar to those in the unsmooth solutions,

again as hoped; but the dependence of orbital fraction on shell number is now more nearly continuous, a result of the smoothness constraint.

These results encourage us to believe that there do exist smooth solutions corresponding to at least some of our unsmooth ones, and that our unsmooth solutions have essentially the same, average properties as the smooth solutions that they are meant to represent.

## 6. DISCUSSION

This investigation may be seen as a logical extension of the work of Richstone, Schwarzschild and collaborators (Richstone 1980, 1982, 1984; Levison & Richstone 1987; Miralda-Escudé & Schwarzschild 1989; Lees & Schwarzschild 1992; Schwarzschild 1993) on the self-consistency problem for scale-free triaxial galaxies. Much of that work was directed toward understanding the constraints that self-consistency places on the shapes of galactic halos. On kiloparsec scales, the orbital times in galactic halos are of order 1% of a Hubble time. Since stochastic orbits do not behave very differently from regular orbits over time scales of  $\sim 100$  oscillations, Schwarzschild (1993) adopted the reasonable point of view that stochastic orbits, integrated for only  $\sim 55$  orbital periods, could safely be included in his solutions without strongly violating the assumption of stationarity. He found that stochastic orbits were often required for self-consistency and showed that their continued evolution over a Hubble time would not seriously compromise his models.

Although the fraction of chaotic phase space is not greatly different in our models than in Schwarzschild's scale-free ones, we have treated the stochastic orbits in a rather different manner. Dynamical time scales near the center of an elliptical galaxy with a cusp are a small fraction of a Hubble time. As a result, the stochastic orbits can diffuse quickly through phase space, causing them to lose their distinguishability in less than a galaxy lifetime. We found that the number of orbital periods required for stochastic orbits to visit their allowed phase-space regions in an effectively ergodic manner is of order  $10^2 - 10^3$  dynamical times in a model with a  $1/r^2$  density cusp, implying that the stars on stochastic orbits near the centers of such galaxies should be distributed with approximately uniform density in their permitted phase space regions. This requirement was shown to be inconsistent with dynamical equilibrium, in the sense that only the innermost 1 or 2 shells of orbits – containing  $\sim 5\%$  of the mass – could be constrained to be fully mixed without violating the self-consistency equations. Even in a typical bright elliptical galaxy, where dynamical time scales are relatively long, one would expect the  $\sim 20\%$  most-bound stars to have undergone more than  $10^3$  orbits during the lifetime of the galaxy (§4.2); and this fraction would be larger in small, dense ellipticals like M32. Thus we conclude that strong triaxiality is difficult or impossible to maintain in a galaxy with a high central concentration of mass.

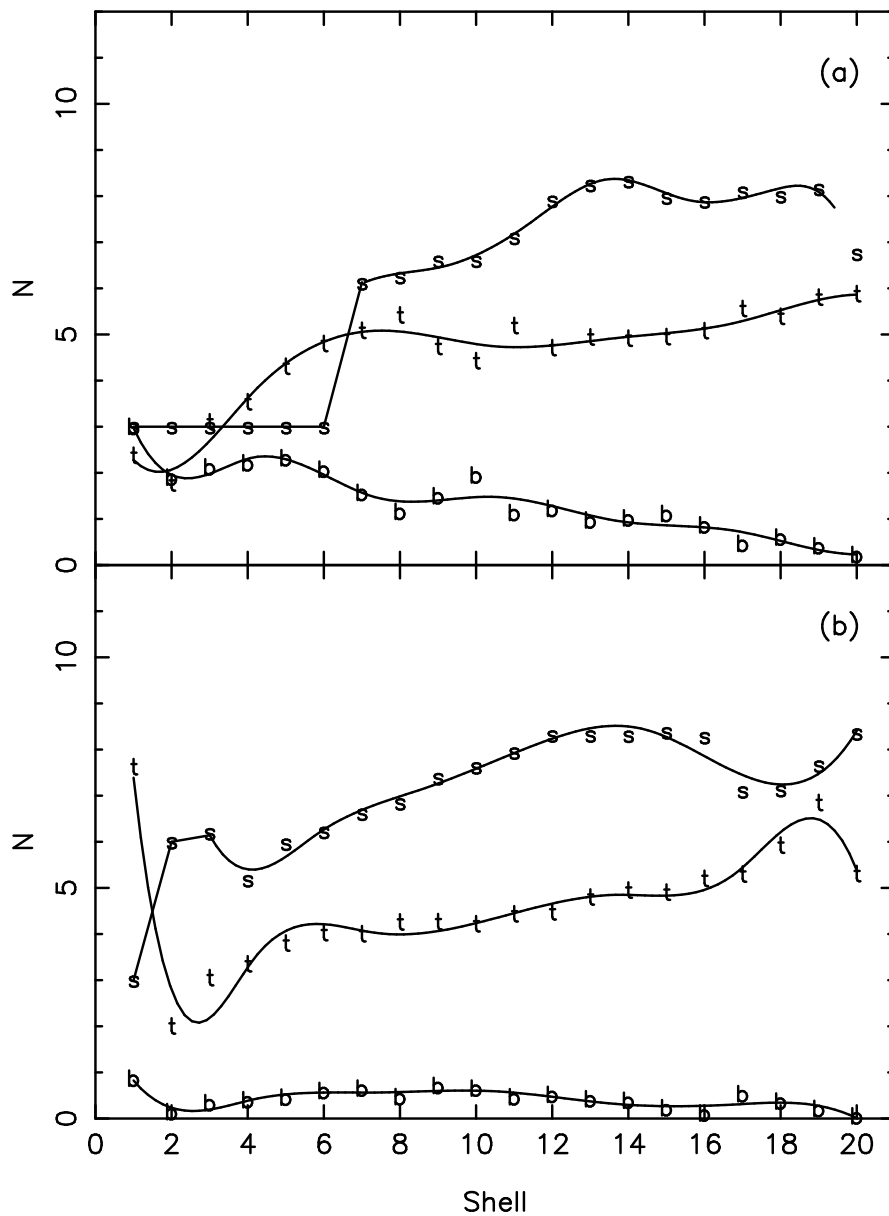


Figure 14. Like Figure 12, for the two smooth solutions indicated in Fig. 13. (a) Weak cusp; (b) strong cusp.

In our weak-cusp model, by contrast, a variety of physically interesting solutions were found, including solutions in which the stochastic orbits were fully mixed, or simply omitted, within approximately the half-mass radius. This greater variety of solutions can be traced to the greater variety of regular orbit families in the weak-cusp potential, which permit less weight to be assigned to the stochastic orbits near the model center. These

models represent galaxies that would evolve very little over a Hubble time, for two reasons: because the stochastic parts of phase space are populated in a nearly time-independent manner at low energies; and because the diffusion time scales for stochastic orbits in the weak-cusp potential are typically very long, of order  $10^3$  dynamical times or more, so that the non-uniform population of stochastic phase space at higher energies would not result in significant evolution over a galaxy lifetime.

Our study raises at least as many questions as it answers. Among these are:

1. *How weak a central cusp can generate significant amounts of stochasticity in a triaxial potential?* One of the surprises of this study was the existence of large numbers of stochastic orbits in triaxial models with density cusps as mild as  $\rho \propto r^{-1}$ . After this study was begun, it was demonstrated that the luminosity densities of Lauer *et al.*'s (1995) “core” galaxies are well described as power laws, with logarithmic slopes ranging from  $-1$  to  $0$  (Merritt & Fridman 1995). It may be shown that the long-axis orbit, which generates regular box orbits in integrable or nearly-integrable triaxial potentials, becomes stable at most energies only when the cusp density increases more slowly than  $r^{-0.5}$  (Merritt & Fridman 1995); thus, bona-fide box orbits can only exist in elliptical galaxies with the weakest observed cusps. It would be interesting to know whether the fraction of stochastic phase space in a triaxial potential remains roughly constant as the cusp slope is reduced to this value, or whether a larger and larger fraction of the phase space becomes regular. Whichever happens, the Liapunov exponents presumably become smaller as the cusp is made weaker, implying less of a role for chaos.

In addition to the mass models discussed here, the family:

$$\rho(m) = \rho_0(1 + m^2)^{-1}(m_0 + m^2)^{-1} \quad (27)$$

would be interesting to investigate in this regard. For  $m_0 = 1$ , equation (27) is the “perfect” law (de Zeeuw 1985), while for  $m_0 = 0$  it is similar to the strong-cusp models presented here. Thus varying the parameter  $m_0$  takes one from a fully integrable (but non-physical) potential to a strongly non-integrable (but realistic) potential.

2. *How would our results have changed if we had adopted a more nearly axisymmetric mass model?* By assuming maximal triaxiality, we forced our solutions to sample heavily from the non-tube orbits, many of which are stochastic. A more nearly oblate or prolate model would have assigned larger weights to the tube orbits and thus might have achieved self-consistency without so strongly occupying the stochastic orbits. Our results imply only that stochasticity is important in strongly triaxial, cuspy galaxies.

3. *Would the addition of a slow figure rotation strongly affect the amount of stochasticity in these models?* Figure rotation is known to induce strong stochasticity at energies near corotation (e.g. Contopoulos 1983). It might conceivably produce an important change in the degree of stochasticity at small radii as well, since the axial orbits that are the generators of stochasticity in our models become elliptical in the presence of rotation, thus tending to avoid the central cusp.

4. *How would the addition of a central point mass affect the triaxial self-consistency problem?* The evidence for central mass concentrations, possibly supermassive black holes, at the centers of some early-type galaxies and bulges of spiral galaxies has recently become very convincing (e.g. Ford *et al.* 1994; Miyoshi *et al.* 1995). Unlike a cusp, a central point mass subjects stars that pass near to it to large-angle scattering. Gerhard & Binney (1985) argued that a central black hole with 2% of the “core” mass would disrupt most box orbits with apocenters interior to about 1 kpc. The phase space of a triaxial model with a mass distribution like that in galaxy M32 – which has a strong cusp and an additional, pointlike mass concentration, possibly a black hole (Tonry 1987) – would be even more dominated by chaos than the models examined here. Significant triaxiality would presumably be very hard to maintain in such a galaxy. In fact, axisymmetric models have proved to be very successful at reproducing the kinematical data for this galaxy (van der Marel *et al.* 1994).

5. *How accurately can the invariant density associated with the stochastic part of phase space at a given energy be approximated by time-averaged trajectories?* There are at least two issues here, one numerical and one physical. A time-averaged regular orbit generates a uniform phase-space density on its KAM torus; this “ergodic” property of regular orbits justifies the use of time-averaged occupation numbers when constructing equilibrium models. No such proof of ergodicity exists for stochastic orbits, and it is at least possible that even an infinitely long integration of such an orbit would not produce a uniform filling of the Arnold web. This possibility is worrisome from the point of view of numerical construction of equilibrium models, but does not seem desperately relevant for real galaxies, which care only about the phase-space distribution at a *given* time. The physically more relevant issue is whether there exist stochastic trajectories that can remain confined to a limited part of stochastic phase space even over very long time scales. Evidence for such “quasi-regular” orbits in the weak-cusp potential was presented in §4.2. Is it fair to populate such orbits with a different density than that of the other parts of stochastic phase space, or would small perturbations quickly cause such orbits to sample the entire Arnold web?

6. *Can elliptical galaxies with cusps reach triaxial steady states like those found here, or would they bypass triaxial configurations in favor of axisymmetric ones?* Our work demonstrates the existence of idealized triaxial models in which the stochastic parts of phase space are populated in an approximately uniform, and hence time-independent, manner. We have not shown that a real galaxy could find these equilibria. A real galaxy might always choose axisymmetry or at best only mild triaxiality, or — particularly in the case of a galaxy with a weak cusp — it might quickly reach a nearly steady, triaxial state and then continue evolving slowly in the direction of axisymmetry, from the inside out. We do not see any obvious way to choose between these possibilities based on the modest number of equilibrium models that we have presented here. Perhaps the only safe

conclusions that we can draw are that chaos and slow evolution are likely to be generic properties of triaxial stellar systems.

The computer programs used in this study for integrating orbits, computing Liapunov exponents and finding and classifying periodic orbits were written by the Geneva group and graciously lent to us by S. Udry and D. Pfenniger. These programs enormously facilitated the work presented here. Ya. G. Sinai devoted several sessions to explaining ergodic theory to us and made a number of suggestions that affected the course of this work. The universal power-law nature of elliptical galaxy nuclei became apparent to us early in 1995, after we had been given pre-publication access to HST surface brightness data by T. Lauer and J. Kormendy. Conversations with D. Pfenniger and O. Gerhard were invaluable for understanding the apparent discrepancy described in §4 between our work and theirs. D. Richstone, J. Sellwood and S. Tremaine sat through extended presentations of this work in its late stages and made numerous comments that improved the final written version. G. Contopoulos, W. Dehnen, H. Kandrup, N. Murray, G. Quinlan and M. Schwarzschild also made comments that improved the presentation. This work was supported by NSF grant AST 90-16515 and by NASA grant NAG 5-2803 to DM.

Table 1  
1 : 1 Resonant Orbits in the  $x$ - $y$  Plane

Shell	Radius <sup>a</sup>		Energy		$T_D$	
	$\gamma = 1$	$\gamma = 2$	$\gamma = 1$	$\gamma = 2$	$\gamma = 1$	$\gamma = 2$
1	0.2791	0.0500	-0.9964	-3.789	2.444	0.160
2	0.4464	0.1053	-0.8670	-2.884	3.381	0.342
3	0.6076	0.1667	-0.7695	-2.359	4.262	0.551
4	0.7744	0.2353	-0.6887	-1.989	5.176	0.790
5	0.9529	0.3125	-0.6186	-1.704	6.167	1.068
6	1.148	0.4000	-0.5562	-1.474	7.274	1.394
7	1.366	0.5000	-0.4997	-1.280	8.538	1.779
8	1.612	0.6154	-0.4478	-1.114	10.01	2.240
9	1.896	0.7500	-0.3998	-0.9695	11.76	2.800
10	2.226	0.9090	-0.3551	-0.8412	13.88	3.489
11	2.620	1.100	-0.3132	-0.7264	16.50	4.356
12	3.097	1.333	-0.2738	-0.6227	19.84	5.471
13	3.690	1.625	-0.2366	-0.5285	24.21	6.945
14	4.449	2.000	-0.2014	-0.4424	30.15	8.964
15	5.458	2.500	-0.1680	-0.3634	38.61	11.86
16	6.866	3.200	-0.1363	-0.2905	51.44	16.28
17	8.974	4.250	-0.1062	-0.2232	72.68	23.64
18	12.48	6.000	-0.0776	-0.1609	112.9	37.64
19	19.49	9.500	-0.0504	-0.1031	209.2	71.26
20	40.49	20.00	-0.0245	-0.0496	596.6	207.3

<sup>a</sup> On  $x$ -axis.



Table 2  
Closed orbits in  $X - Z$  start space: Model 1 ( $\gamma = 1$ )

N	Resonance	Family	Shell	$x_0$	$y_0$	$z_0$	Stability
1	1:1:S	xy-loop	1	0.14773	0.	0.	st
			2	0.24051	0.	0.	st
			3	0.33037	0.	0.	st
			4	0.42306	0.	0.	st
			5	0.52171	0.	0.	st
			6	0.62894	0.	0.	st
			7	0.74747	0.	0.	st
			8	0.88052	0.	0.	st
			9	1.03217	0.	0.	st
			10	1.20781	0.	0.	st
			11	1.41488	0.	0.	st
			12	1.66403	0.	0.	st
			13	1.97118	0.	0.	st
			14	2.36126	0.	0.	st
			15	2.87578	0.	0.	st
			16	3.58944	0.	0.	st
			17	4.65167	0.	0.	st
			18	6.41142	0.	0.	st
			19	9.91654	0.	0.	st
			20	20.41194	0.	0.	st
2	S:1:1	yz-loop	1	0.	0.	0.16602	st
			2	0.	0.	0.25916	st
			3	0.	0.	0.34662	st
			4	0.	0.	0.43549	st
			5	0.	0.	0.52941	st
			6	0.	0.	0.63121	st
			7	0.	0.	0.74378	st
			8	0.	0.	0.87042	st
			9	0.	0.	1.01526	st
			10	0.	0.	1.18375	st
			11	0.	0.	1.38342	st
			12	0.	0.	1.62499	st
			13	0.	0.	1.92448	st
			14	0.	0.	2.30701	st
			15	0.	0.	2.81433	st
			16	0.	0.	3.52158	st
			17	0.	0.	4.57891	st
			18	0.	0.	6.33655	st
			19	0.	0.	9.84490	st
			20	0.	0.	20.35492	st

Table 3  
Closed orbits in stationary start space: Model 1 ( $\gamma = 1$ )

N	Resonance	Family	Shell	$x_0$	$y_0$	$z_0$	Stability
3	1:2:S	xy-banana	1	0.2791	0.0001	0.	v
4	1:S:2	xz-banana	1	0.2754	0.	0.0329	st
			2	0.4382	0.	0.0622	st
			3	0.5937	0.	0.0959	st
			4	0.7530	0.	0.1355	st
			5	0.9222	0.	0.1823	st
			6	1.1058	0.	0.2379	st
			7	1.3089	0.	0.3041	st
			8	1.5371	0.	0.3836	st
			9	1.7977	0.	0.4798	st
			10	2.1003	0.	0.5973	st
			11	2.4581	0.	0.7428	st
			12	2.8900	0.	0.9258	st
			13	3.4243	0.	1.1610	st
			14	4.1054	0.	1.4713	st
			15	5.0069	0.	1.8951	st
			16	6.2613	0.	2.5021	st
			17	8.3135	0.	3.4323	st
			18	11.2411	0.	5.0138	st
			19	17.4355	0.	8.2351	st
			20	35.9663	0.	18.0606	st
5	S:1:2	yz-banana	1	0.	0.2484	0.0043	v
6	2:3:S	xy-fish	1	0.2777	0.0246	0.	v
7	2:S:3	xz-fish	1	0.1896	0.	0.0329	st
			2	0.2961	0.	0.2487	st
			3	0.3947	0.	0.3495	st
			4	0.4932	0.	0.4584	st
			5	0.5954	0.	0.5793	st
			6	0.7041	0.	0.7160	st
			7	0.8220	0.	0.8729	v
8	S:2:3	yz-fish	1	0.	0.2251	0.0865	v
9	3:4:S	pretzel	1	0.2346	0.1343	0.	st
			2	0.3560	0.2404	0.	st
			3	0.4627	0.3536	0.	st
			4	0.5644	0.4784	0.	st
			5	0.6654	0.6183	0.	st
			6	0.7688	0.7767	0.	st
			7	0.8767	0.9583	0.	st
			8	0.9919	1.1683	0.	st
			9	1.1171	1.4142	0.	st

		10	1.2560	1.7059	0.	v
10	3:4:6	10	1.2691	1.6875	0.1629	st
		11	1.4444	2.0133	0.2835	st
		12	1.6509	2.4102	0.4264	st
		13	1.9006	2.9051	0.6082	st
		14	2.2124	3.5399	0.8493	st
		15	2.6173	4.3850	1.1825	st
		16	3.1716	5.5662	1.6659	st
		17	3.9864	7.3362	2.4161	st
		18	5.3205	10.2838	3.7074	st
		19	7.9492	16.1746	6.3681	st
		20	15.7302	33.8365	14.5659	st
11	4:5:S	1	0.1668	0.1990	0.	v
12	4:5:7	1	0.1669	0.1987	0.0061	st
		2	0.2459	0.3288	0.0446	st
		3	0.3124	0.4572	0.0858	st
		4	0.3737	0.5916	0.1350	st
		5	0.4330	0.7361	0.1942	u
13	5:6:S	1	0.1126	0.2272	0.	st
		2	0.1566	0.3741	0.	st
		3	0.1890	0.5196	0.	st
		4	0.2157	0.6725	0.	st
		5	0.2388	0.8380	0.	v
14	5:6:8	1	0.1229	0.1941	0.0900	st
		2	0.1756	0.3124	0.1607	st
		3	0.2172	0.4257	0.2371	st
		4	0.2537	0.5427	0.3228	st
		5	0.2873	0.6642	0.4205	st
		6	0.3196	0.7965	0.5331	st
		7	0.3515	0.9418	0.6642	st
		8	0.3843	1.1041	0.8184	st
		9	0.4184	1.2884	1.0017	st
		10	0.4554	1.5010	1.2223	st
		11	0.4963	1.7509	1.4917	st
		12	0.5433	2.0510	1.8265	u
15	5:6:9	5	0.2398	0.8372	0.0259	st
		6	0.2672	1.0141	0.0864	st
		7	0.2946	1.2111	0.1458	st
		8	0.3227	1.4337	0.2162	st
		9	0.3525	1.6887	0.3027	st
		10	0.3846	1.9857	0.4106	st
		11	0.4204	2.3376	0.5470	st
		12	0.4610	2.7629	0.7220	st

		13	0.5093	3.2895	0.9507	st
		14	0.5680	3.9610	1.2568	u
16	5:7:8	6	0.8225	0.1690	0.6112	u
		7	0.9495	0.2252	0.7559	st
		8	1.0867	0.2897	0.9262	st
		9	1.2378	0.3638	1.1290	st
		10	1.4075	0.4495	1.3734	st
		11	1.6022	0.5494	1.6725	st
		12	1.8313	0.6679	2.0446	u
17	6:7:9	1	0.0896	0.1687	0.1353	st
		2	0.1239	0.2685	0.2295	st
		3	0.1487	0.3621	0.3277	st
		4	0.1688	0.4559	0.4353	st
		5	0.1859	0.5533	0.5559	st
		6	0.2012	0.6570	0.6932	st
		7	0.2155	0.7694	0.8513	st
		8	0.2294	0.8937	1.0352	st
		9	0.2435	1.0336	1.2520	u
18	7:5:12	6	0.9421	0.1479	0.4950	u
		7	1.0969	0.2167	0.6144	st
		8	1.2648	0.3010	0.7556	st
		9	1.4498	0.4030	0.9249	st
		10	1.6571	0.5265	1.1307	st
		11	1.8939	0.6766	1.3845	st
		12	2.1705	0.8608	1.7031	st
		13	2.4943	1.0872	2.1032	st
		14	2.9119	1.3850	2.6490	st
		15	3.4416	1.7748	3.3830	u
19	7:8:10	1	0.0631	0.1425	0.1619	st
		2	0.0837	0.2240	0.2706	st
		3	0.0967	0.2980	0.3822	st
		4	0.1059	0.3701	0.5034	st
		5	0.1128	0.4428	0.6383	st
		6	0.1180	0.5182	0.7909	u
20	7:9:10	1	0.1425	0.0390	0.1735	st
		2	0.2133	0.0700	0.2881	st
		3	0.2727	0.0993	0.4053	st
		4	0.3272	0.1275	0.5323	st
		5	0.3795	0.1547	0.6735	st
		6	0.4313	0.1811	0.8330	st
		7	0.4840	0.2072	1.0155	st
		8	0.5389	0.2334	1.2269	st
		9	0.5973	0.2600	1.4747	u

Table 4  
Closed orbits in  $X - Z$  start space: Model 2 ( $\gamma = 2$ )

N	Resonance	Family	Shell	$x_0$	$y_0$	$z_0$	Stability
1	1:1:S	xy-loop	1	0.02752	0.	0.	st
			2	0.05786	0.	0.	st
			3	0.09147	0.	0.	st
			4	0.12891	0.	0.	st
			5	0.17087	0.	0.	st
			6	0.21821	0.	0.	st
			7	0.27205	0.	0.	st
			8	0.33386	0.	0.	st
			9	0.40556	0.	0.	st
			10	0.48979	0.	0.	st
			11	0.59024	0.	0.	st
			12	0.71221	0.	0.	st
			13	0.86366	0.	0.	st
			14	1.05706	0.	0.	st
			15	1.31320	0.	0.	st
			16	1.66945	0.	0.	st
			17	2.20056	0.	0.	st
			18	3.08103	0.	0.	st
			19	4.83472	0.	0.	st
			20	10.08362	0.	0.	st
2	S:1:1	yz-loop	1	0.	0.	0.02719	st
			2	0.	0.	0.05703	st
			3	0.	0.	0.08995	st
			4	0.	0.	0.12649	st
			5	0.	0.	0.16733	st
			6	0.	0.	0.21333	st
			7	0.	0.	0.26560	st
			8	0.	0.	0.32559	st
			9	0.	0.	0.39522	st
			10	0.	0.	0.47712	st
			11	0.	0.	0.57496	st
			12	0.	0.	0.69406	st
			13	0.	0.	0.84238	st
			14	0.	0.	1.03244	st
			15	0.	0.	1.28509	st
			16	0.	0.	1.63786	st
			17	0.	0.	2.16581	st
			18	0.	0.	3.04403	st
			19	0.	0.	4.79770	st
			20	0.	0.	10.05232	st

Table 5  
Closed orbits in stationary start space: Model 2 ( $\gamma = 2$ )

N	Resonance	Family	Shell	$x_0$	$y_0$	$z_0$	Stability
3	1:2:S	xy-banana	1	0.0478	0.0135	0.0000	v
4	1:S:2	xz-banana	1	0.0440	0.	0.0186	st
			2	0.0923	0.	0.0396	st
			3	0.1459	0.	0.0636	st
			4	0.2055	0.	0.0911	st
			5	0.2717	0.	0.1224	st
			6	0.3477	0.	0.1596	st
			7	0.4336	0.	0.2027	st
			8	0.5323	0.	0.2535	st
			9	0.6471	0.	0.3142	st
			10	0.7822	0.	0.3876	st
			11	0.9439	0.	0.4775	st
			12	1.1408	0.	0.5899	st
			13	1.3613	0.	0.7681	st
			14	1.7009	0.	0.9216	st
			15	2.1194	0.	1.1775	st
			16	2.7036	0.	1.5429	st
			17	3.5778	0.	2.1012	st
			18	5.0315	0.	3.0481	st
			19	7.9320	0.	4.9734	st
			20	16.6130	0.	10.8368	st
5	S:1:2	yz-banana	1	0.	0.0427	0.0144	v
6	2:3:S	xy-fish	1	0.0358	0.0319	0.	v
7	2:S:3	xz-fish	1	0.0233	0.	0.0353	v
8	S:2:3	yz-fish	1	0.	0.0284	0.0314	v
9	3:4:6		1	0.0264	0.0344	0.0155	st
			2	0.0549	0.0727	0.0335	st
			3	0.0856	0.1156	0.0543	st
			4	0.1190	0.1640	0.0785	st
			5	0.1556	0.2188	0.1070	st
			6	0.1959	0.2811	0.1405	st
			7	0.2407	0.3529	0.1804	st
			8	0.2909	0.4360	0.2283	st
			9	0.3479	0.5334	0.2863	st
			10	0.4134	0.6489	0.3574	st
			11	0.4895	0.7874	0.4455	st
			12	0.5807	0.9580	0.5578	st
			13	0.6913	1.1710	0.7026	st
			14	0.8300	1.4448	0.8951	st

		15	1.0099	1.8101	1.1600	st
		16	1.2558	2.3210	1.5424	st
		17	1.6160	3.0862	2.1330	st
		18	2.2031	4.3588	3.1445	st
		19	3.3525	6.8965	5.2190	st
		20	6.7336	14.4866	11.5849	u
10	4:5:7	1	0.0131	0.0345	0.0238	st
		2	0.0268	0.0728	0.0512	st
		3	0.0410	0.1149	0.0827	st
		4	0.0559	0.1619	0.1190	st
		5	0.0720	0.2144	0.1613	st
		6	0.0890	0.2737	0.2106	st
		7	0.1074	0.3410	0.2688	st
		8	0.1274	0.4183	0.3379	st
		9	0.1494	0.5078	0.4209	st
		10	0.1739	0.6130	0.5215	st
		11	0.2015	0.7383	0.6455	u
11	4:6:7	1	0.0325	0.0106	0.0286	st
		2	0.0677	0.0225	0.0612	st
		3	0.1058	0.0359	0.0984	st
		4	0.1474	0.0512	0.1414	st
		5	0.1929	0.0685	0.1910	u
12	5:7:8	1	0.0253	0.0105	0.0331	st
		2	0.0522	0.0220	0.0706	st
		3	0.0812	0.0346	0.1136	st
		4	0.1126	0.0483	0.1628	st
		5	0.1467	0.0636	0.2195	st
		6	0.1840	0.0805	0.2852	st
		7	0.2252	0.0994	0.3621	st
		8	0.2713	0.1206	0.4527	st
		9	0.3234	0.1446	0.5606	st
		10	0.3831	0.1723	0.6906	st
		11	0.4527	0.2045	0.8495	u

## 7. REFERENCES

- Aarseth, S. J. & Binney, J. J. 1978, MNRAS, 185, 227
- Arnold, V. I. 1964, Russian Math. Surveys 18, 85
- Benettin, G., Galgani, L., Giorgilli, A. & Strelcyn, J.-M. 1980, Meccanica 15, 21
- Binney, J. J. 1982a, MNRAS, 201, 1
- Binney, J. J. 1982b, MNRAS, 201, 15
- Binney, J. J. 1987, in IAU Symposium No. 127, Structure and Dynamics of Elliptical Galaxies, ed. T. de Zeeuw (Dordrecht: Reidel), p. 269
- Carollo, C. M. 1993, Ph.D. thesis, Ludwig-Maximilians Univ., Munich
- Chandrasekhar, S. 1969, Ellipsoidal Figures of Equilibrium (New York: Dover), p. 52
- Chirikov, B. V. 1979, Phys. Rept. 52, 263
- Contopoulos, G. 1983, A&A, 117, 89
- Contopoulos, G. & Barbanis, B. 1989, A&A, 222, 329
- Crane, P. *et al.* 1993, AJ, 106, 1371
- Crone, M., Evrard, A. E. & Richstone, D. O. 1994, ApJ, 434, 402
- Dehnen, W. 1993, MNRAS, 265, 250
- de Zeeuw, P. T. 1985, MNRAS, 216, 273
- de Zeeuw, P. T. & Lynden-Bell, D. 1985, MNRAS, 215, 713
- de Zeeuw, P. T. & Pfenniger, D. 1988, MNRAS, 235, 949
- Fehlberg, E. 1968, NASA Technical Report TR R-287
- Ferrarese, L., van den Bosch, F. C., Ford, H. C., Jaffe, W., & O'Connell, R. W. 1994, AJ, 108, 1598
- Ford, H. C. *et al.* 1994, ApJ, 435, L27
- Gebhardt, K. *et al.* 1996, preprint.
- Gebhardt, K., Richstone, D. O. *et al.* 1996, preprint
- Gerhard, O. E. 1987, in IAU Symposium No. 127, Structure and Dynamics of Elliptical Galaxies, ed. T. de Zeeuw (Dordrecht: Reidel), p. 241
- Gerhard, O. E. & Binney, J. J. 1985, MNRAS, 216, 467
- Goodman, J. & Schwarzschild, M. 1981, ApJ, 245, 1087
- Heggie, D. 1991, in Predictability, Stability and Chaos in *N*-Body Dynamical Systems, ed. A. E. Roy (New York: Plenum), p. 47.
- Henon, M. & Heiles, C 1964, AJ, 69, 73
- Hernquist, L. 1990, ApJ, 356, 359
- Jaffe, W. 1983, MNRAS, 202, 995
- Jaffe, W., Ford, H. C., O'Connell, R. W. van den Bosch, F. C. & Ferrarese, L. 1994, AJ, 108, 1567
- Jaynes, E. T. 1984, in Inverse Problems, ed. D. W. McLaughlin (Providence: SIAM), p. 151
- Kormendy, J. 1985, ApJ, 292, L9
- Kormendy, J., Dressler, A., Byun, Y.-I., Faber, S. M., Grillmair, C., Lauer, T. R., Rich-



- stone, D., & Tremaine, S. 1995, in ESO/OHP Workshop on Dwarf Galaxies, ed. G. Meylan & P. Prugniel (Garching: ESO), p. 147
- Kuijken, K. 1993, ApJ, 409, 68
- Kuzmin, G. G. 1973, in The Dynamics of Galaxies and Star Clusters, ed. T. B. Omarov (Nauka of the Kazakh S. S. R., Alma-Ata), p. 71.
- Lauer, T. *et al.* 1995, preprint.
- Lees, J. F. & Schwarzschild, M. 1992, ApJ, 384, 491
- Levison, H. F. & Richstone, D. O. 1987, ApJ, 314, 476
- Lichtenberg, A. J. & Lieberman, M. A. 1992, Regular and Chaotic Dynamics (New York: Springer)
- Lynden-Bell, D. 1967, MNRAS, 136, 101
- Merritt, D. 1996, *Cel. Mech.*, in press
- Merritt, D. & Fridman, T. 1995, in Fresh Views of Elliptical Galaxies, ed. A. Buzzoni, A. Renzini & A. Serrano, in press
- Miller, G.F. 1974, in Numerical Solutions of Integral Equations, ed. L.M. Delves & J. Walsh (Oxford: Clarendon), p.175
- Miralda-Escudé, J. & Schwarzschild, M. 1989, ApJ, 339, 752
- Miyoshi, M. *et al.* 1995, Nature 373, 127
- Moller, P., Stiavelli, M. & Zeilinger, W. W. 1995, MNRAS, 276, 979
- Nieto, J.-L. & Bender, R. 1989, A&A, 215, 266
- O'Sullivan, F. 1986, *Stat. Sci.* 1, 502
- Pfenniger, D. & de Zeeuw, T. 1989, in Dynamics of Dense Stellar Systems, ed. D. Merritt (Cambridge: Cambridge), p. 81
- Phillips, D. L. 1962, J. Ass. Comput. Mach. 9, 84
- Richstone, D. O. 1980, ApJ, 238, 103
- Richstone, D. O. 1982, ApJ, 252, 496
- Richstone, D. O. 1984, ApJ, 281, 100
- Richstone, D. O. & Tremaine, S. 1988, ApJ, 327, 82
- Schwarzschild, M. 1979, ApJ, 232, 236
- Schwarzschild, M. 1982, ApJ, 263, 599
- Schwarzschild, M. 1993, ApJ, 409, 563
- Sinai, Ya. G. 1976, Introduction to Ergodic Theory (Princeton: Princeton University Press)
- Statler, T. S. 1987, ApJ, 321, 113
- Tikhonov, A. N. 1963, Soviet Math. 4, 1035
- Tonry, J. L. 1987, ApJ, 322, 632
- Tremaine, S., Richstone, D., Buyn, Y.-I., Dressler, A., Faber, S. M., Grillmair, C., Kormendy, J., & Lauer, T. R. 1994, AJ, 107, 634
- Tremaine, S., Henon, M. & Lynden-Bell, D. 1986, MNRAS, 219, 285
- Udry, S. & Pfenniger, D. 1988, A&A, 198, 135

van der Marel, R. P., Evans, N. W., Rix, H. W., White, S. & de Zeeuw, T. 1994, MNRAS, 271, 99

Wilkinson, A. & James, R. A. 1982, MNRAS, 199, 171